Atmos. Chem. Phys. Discuss., 13, 17849–17900, 2013
www.atmos-chem-phys-discuss.net/13/17849/2013/
doi:10.5194/acpd-13-17849-2013

Atmospheric Chemistry and Physics Discussions

Drift-corrected trends and periodic variations in MIPAS IMK/IAA ozone measurements

E. Eckert[1], T. von Clarmann[1], M. Kiefer[1], G. P. Stiller[1], S. Lossow[1], N. Glatthor[1], D. A. Degenstein[2], L. Froidevaux[3], S. Godin-Beekmann[4], T. Leblanc[5], S. McDermid[5], M. Pastel[4], W. Steinbrecht[6], D. P. J. Swart[7], K. A. Walker[8], and P. F. Bernath[9]

[1]Karlsruhe Institute of Technology, Institute for Meteorology and Climate Research, Karlsruhe, Germany
[2]Institute of Space and Atmospheric Studies, University of Saskatchewan, Saskatoon, Canada
[3]CalTech/Jet Propulsion Laboratory, Pasadena, California
[4]Laboratoire Atmosphère, Milieux, Observations Spatiales (LATMOS), Institut Pierre Simon Laplace, Université Pierre et Marie Curie, Université Versailles St-Quentin-en-Yvelines, Centre National de la Recherche Scientifique, Paris, France
[5]California Institute of Technology, Jet Propulsion Laboratory, Wrightwood, CA, USA
[6]Meteorological Observatory, Deutscher Wetterdienst, Hohenpeissenberg, Germany
[7]National Institute of Public Health and Environmental Protection, P.O. Box 1, NL-3720 BA Bilthoven, the Netherlands
[8]Department of Physics, University of Toronto, Ontario, Canada

[9]Department of Chemistry and Biochemistry, Old Dominion University, Norfolk, VA 23529-0126, USA

Received: 7 June 2013 – Accepted: 18 June 2013 – Published: 4 July 2013

Correspondence to: E. Eckert (ellen.eckert@kit.edu)

Published by Copernicus Publications on behalf of the European Geosciences Union.

ACPD
13, 17849–17900, 2013

Abstract

Drifts, trends and periodic variations were calculated from monthly zonally averaged ozone profiles. The ozone profiles, among many other species, were derived from level-1b data of the Michelson Interferometer for Passive Atmospheric Sounding (MIPAS) by means of the scientific level-2 processor run by Karlsruhe Institute of Technology (KIT), Institute for Meteorlogy and Climate Research (IMK). All trend and drift analyses were performed using a multilinear parametric trend model which includes a linear term, several harmonics with period lengths from three to twenty four months and the quasi-biennial oscillation (QBO). Drifts at 2-sigma significance level were mainly negative for ozone relative to Aura MLS and Odin OSIRIS and negative or near zero for most of the comparisons to Lidar measurements. Lidar stations used here include those at Hohenpeissenberg (47.8° N, 11.0° E), Lauder (45.0° S, 169.7° E), Mauna Loa (19.5° N, 155.6° W), Observatoire Haute Provence (43.9° N, 5.7° E) and Table Mountain (34.4° N, 117.7° W). Drifts against ACE-FTS were found to be mostly insignificant. The assessed MIPAS ozone trends cover the time period of July 2002 to April 2012 and range from $-0.5\,\mathrm{ppmv\,decade^{-1}}$ to $+0.5\,\mathrm{ppmv\,decade^{-1}}$ depending on altitude and latitude. From the drift analyses we derive that the real ozone trends might be slighly more positive/less negative than those calculated from the MIPAS data, by conceding the possibility of MIPAS having a very small (approx. within $-0.3\,\mathrm{ppmv\,decade^{-1}}$) negative drift for ozone. This leads to drift-corrected trends of $-0.4\,\mathrm{ppmv\,decade^{-1}}$ to $+0.55\,\mathrm{ppmv\,decade^{-1}}$ for the time period covered by MIPAS Envisat measurements with very few negative and large areas of positive trends, which is in good agreement with recent literature. Differences of the trends compared with recent literature could be explained by a possible shift of the subtropical mixing barriers. Results for the altitude-latitude distribution of amplitudes of the quasi-biennial, annual and the semi-annual oscillation are also in very good agreement with recent findings.

ACPD
13, 17849–17900, 2013

1 Introduction

Stratospheric ozone depletion has been an important issue for more than the past three decades. Although ozone can cause health problems when being present close to the surface in unnaturally large amounts, e.g. in the downstream of urban areas during warm periods, its presence is very important at higher altitudes. Most of the ozone is located in the stratosphere, where it absorbs ultraviolet light coming from the sun. Light at these wavelengths can lead to e.g. increased risk of skin cancer, hence the careful monitoring of stratospheric ozone abundances is mandatory.

After Hartley's approximate measurements of the absorption of ozone in the ultraviolet Fabry and Buisson were the first to estimate the vertical thickness of ozone in the atmosphere (Dobson, 1968). Shortly afterwards, during the 1920s, Dobson measured column ozone at Oxford using a Féry spectrograph (Dobson, 1931; Götz et al., 1934). Subsequently further Féry spectrographs were set up at several other locations in Europe. As a second step the measurements were expanded beyond Europe during the late 1920's, including a southern hemispheric site at Christchurch, New Zealand. Over the years, many different instruments and measurement techniques were developed so that nowadays data are collected by ground based instruments like lidars, airborne observations including instruments carried by airplanes or balloons and spaceborne limb sounders like MIPAS Envisat, the Microwave Limb Sounder on the Aura satellite (Aura MLS), the Optical Spectrograph and Infrared Imaging System (Odin OSIRIS) and the Atmospheric Chemistry Experiment Fourier Transform Spectrometer (ACE-FTS). Measurements form the latter satellite instruments are used in the analyses that follow.

All measurements show that the largest abundance of ozone can be found in the stratosphere, forming the ozone layer. This layer protects the earth's flora and fauna from most of the harmful solar ultraviolet radiation. Molina and Rowland (1974) discovered that some anthropogenically produced chemicals could lead to the depletion of stratospheric ozone. The discovery of the Antarctic ozone hole by Farman et al. (1985) indicated that ozone depletion due to anthropogenic emission of e.g. chloroflourocar-

ACPD
13, 17849–17900, 2013

bons (CFC) had the potential of a global threat. These findings led to the restriction of major ozone depleting substances (ODSs) via the Montreal Protocol in 1987, but since most of these substances are long-lived their amounts continued to increase in the stratosphere until the mid-90s (WMO, 2011). Consequently a negative global trend in ozone was observed for the same time period, reaching minimum total ozone values during 1996–1997. Even though a decrease of stratospheric ODS concentrations was noted from the mid-1990s on, ozone did not recover consistently. Trends after 1995 were found to be either nonexistent or slightly positive (Steinbrecht et al., 2009a; WMO, 2011).

In this paper, linear variations of ozone calculated from zonal monthly means are shown which were derived from MIPAS Envisat IMK/IAA level-2 V3O_O3_9, V5R_O3_220 and V5R_O3_221 data. The analyses cover the altitude range from 10 to 44 km in steps of one kilometer and continue in 2 km steps up to 50 km. Additionally, altitude-latitude distributions of the amplitude of periodic variations with period lengths of 6 (semi-annual oscillation – SAO) and 12 (annual oscillation – AO) months were assessed, as well as the quasi-biennial oscillation (QBO). These results were obtained using MIPAS data from July 2002 to April 2012. MIPAS measurement data exhibit a gap between March 2004 and January 2005, during which no data could be collected by the instrument due to technical problems. This also led to an altered operation mode for the second time period, with different spectral and horizontal resolution and tangent height pattern.

In order to support the trend analyses, drifts are estimated via comparison with several coincident measurements of space borne instruments, namely ACE-FTS, Aura MLS and Odin OSIRIS. We also calculated drifts comparing MIPAS profiles to coincident measurements of the Network for the Detection of Atmospheric Composition Change (NDACC) lidars at Hohenpeissenberg, Mauna Loa, Lauder, Observatoire Haute Provence and Table Mountain. Our conclusions from the drift analyses were used to correct trends derived from the MIPAS data. The instruments used for this study are introduced and characterized in Sect. 2, followed by a detailed description

ACPD
13, 17849–17900, 2013

of the method of trend estimation and additional scientific tools in Sect. 3. While the results are presented in Sect. 4, we provide a closing overview in the conclusions (Sect. 5), putting the findings of this work into an overall context and point out possible future work.

2 Instruments

2.1 MIPAS Envisat

MIPAS was one of the core payload atmospheric chemistry instruments aboard the European satellite Envisat (Fischer et al., 2008). The satellite was launched into a sun-synchronous polar orbit at approximately 800 km, with 98.55° inclination, by the European Space Agency (ESA) in March 2002. The instrument setup allows global coverage from pole to pole. Envisat crossed the equator at approximately 10:00 and 22:00 LT and performed about 14.4 orbits per day. However it ceased sending data on 8 April 2012 and was declared dead shortly afterwards, so MIPAS provided data for a period of about 10 yr.

MIPAS is a Fourier transform limb emission spectrometer, which measures the signatures of various trace gases within the spectral range of 4.15 to 14.6 µm. Originally (high spectral resolution period), MIPAS measured one limb scan consisting of 17 tangent altitudes from 6 to 68 km and about 75 profiles per orbit in its nominal mode, which results in approximately 1000 profiles per day. The spectral resolution of MIPAS during this first time period (2002–2004) was 0.025 cm^{-1} unapodized (0.035 cm^{-1} apodized). The data product used in this study associated with this time period is the V3O_O3_9 data set. It was developed by improvement of the V3O_O3_7 data using version 4.6x level-1b data set as characterized by Glatthor et al. (2006) and consists of 486 945 ozone profiles. The retrieval grid width in all MIPAS data versions is 1 km for altitudes below 44 km and 2 km above, independent of the tangent altitudes of the measurements. Changes from the V3O_O3_7 described there to the more recent V3O_O3_9

ACPD
13, 17849–17900, 2013

retrieval and processing setup include a switchoff of the first microwindow (741.675 to 741.825 cm^{-1}) at 18 km (Glatthor et al., 2006, Table 1) and the additional usage of the horizontal temperature gradient fitted at a preceding retrieval. The vertical resolution of the V3O_O3_9 version ranges from 3.5 to 5 km between 10 and 40 km (Steck et al., 2007) and becomes slightly coarser above, depending on atmospheric conditions.

For the second time period we chose to use the combination of the V5R_O3_220 (1541 474 profiles) and V5R_O3_221 (331 287 profiles) MIPAS ozone product, both of which were derived from version 5.0 and later level-1b data. The V5R_O3_221 data ozone set consistently extends the V5R_O3_220 product after April 2011. These versions of the ozone product are closely linked with version V4O_O3_202 (deduced from version 4.67 level-1b data) as characterised by von Clarmann et al. (2009) and validated by Stiller et al. (2012b). The thorough validation of the V5R_O3_220 (and V5R_O3_221) is currently in progress (Laeng et al. and paper in preparation). Differences in the setup from version V4O_O3_202 to both V5R_O3 versions are major changes in level 1b data and the temperature fitted in a preceding retrieval. Additionally the upper end of the jointly retrieved continuum profile was shifted from 33 km to 50 km. From version V5R_O3_220 to V5R_O3_221 only minor changes were applied which do not appreciably change the results for ozone in the investigated altitude range. The vertical resolution of the version V5R_O3_220 and V5R_O3_221 data product ranges from about 2.5 to 5 km, exhibiting the worst vertical resolution around 30 to 35 km. Recent investigations of this feature showed that the vertical resolution in this altitude range would be significantly improved by activating microwindows in the MIPAS AB band (1020–1170 cm^{-1}) at and above 33 km instead of 36 km and above as performed for the dataset used here, at the cost of a higher positive bias, however. The combined data set of V3O_O3_9, V5R_O3_220 and V5R_O3_221 contains 2 359 706 ozone profiles in total.

ACPD
13, 17849–17900, 2013

2.2 Aura MLS

The Microwave Limb Sounder (MLS) is one amongst four instruments currently operating on the Earth Observing System (EOS) Aura satellite, which was launched into a sun-synchronous, near-polar orbit at about 705 km by NASA on 15 July 2004. The Aura satellite is dedicated to chemical constituents of the atmosphere, while the other satellites of the EOS program, Aqua and Terra, focus on the hydrological cycle and land processes, respectively (Schoeberl et al., 2006). Aura MLS records microwave emissions in spectral regions centered at approximately 118, 190, 240 and 640 GHz and additionally 2.5 THz (Waters et al., 2006). With a vertical resolution of 2.5 to 3 km it measures atmospheric constituents in the upper troposphere, stratosphere and mesosphere, while achieving nearly pole to pole coverage (82° S to 82° N).

Mainly focussing on tropospheric and stratospheric processes concerning ozone chemistry, Aura MLS provides data on several atmospheric chemical species linked to ozone destruction, including various reservoir gases. With approximately 240 profiles per orbit (nearly 3500 profiles per day) Aura MLS provides a large number of profiles (day and night) and is thus a very good candidate for drift estimation by means of coinciding profiles. In this study the ozone version v2.2 of the Aura MLS data was used. The standard ozone product, which is used in this study, is derived from the 240 GHz region (main line at 235.7 GHz and lines at 243.45 GHz and 244.16 GHz, Froidevaux et al., 2008). This Aura MLS dataset is recommended for pressure levels between 215 and 0.02 hPa, after necessary data screening is applied (Froidevaux et al., 2008). Since the application of the MIPAS averaging kernel, as described in Sect. 3.2.2, was performed on the MIPAS altitude grid we interpolated the Aura MLS data from its pressure grid to an adequate altitude grid using coincident ECMWF temperatures and pressure to calculate pressure-altitude relations.

ACPD
13, 17849–17900, 2013

2.3 ACE-FTS

The Fourier Transform Spectrometer (FTS) of the Atmospheric Chemistry Experiment (ACE) is one of the two instruments on board the Canadian satellite SCISAT-1. It was launched into a circular low-earth orbit at approximately 650 km from an airplane on 12 August 2003 and the routine measurements were started in February 2004. ACE typically measures in the altitude range from 10 to 100 km, depending on the measurement and the strength of the spectral lines, although the high-resolution (0.02 cm^{-1}) infrared FTS can generally start at the cloud tops and reach up to about 150 km. The vertical resolution of the FTS is approximately 3–4 km (Dupuy et al., 2009). While using a similar wavelength region (2.2 to 13.3 µm) as MIPAS, ACE-FTS measures in solar occultation. For this study, the updated version v2.2 of the ACE-FTS ozone data was used for comparison. Due to the fact that some of the profiles seemed to show very unrealistic values, the following rejection criteria were applied: First, the criteria provided at the data issue page (https://databace.scisat.ca/validation/data_issues_table.php), where certain peculiarities are reported, were used to sort out some profiles. Since this approach still left some suspicious profiles in the data sets, we also removed those for which the ozone mixing ratios were outside of the range −10 to 20 ppmv. This range was suggested by Dupuy et al. (2009) during the validation of the ACE-FTS ozone product. The profiles were rejected, if their values were outside these ranges at any point between 0 and 60 km.

2.4 Odin OSIRIS

The Optical Spectrograph and InfraRed Imaging System (OSIRIS) is a Canadian instrument aboard the Swedish Satellite Odin and has been collecting data since February 2001 (Degenstein et al., 2009). It orbits sun-synchronously at about 600 km with northward equator crossing time at 6 p.m. LT and 98° inclination. Since OSIRIS is an instrument which measures scattered sunlight, measurements are only possible during June, July, August and September (November, December, January and February)

ACPD
13, 17849–17900, 2013

at the Northern Hemisphere (Southern Hemisphere) , because sunlight is imperative for the instrument's observations. While the optical spectrograph (OS) records spectra of limb scattered sunlight from 280 to 800 nm and has a spectral resolution of about 1 nm, the second part of the instrument, the infrared imager (IRI), measures scattered sunlight as well as airglow emissions (Llewellyn et al., 2004). The altitudinal coverage of OSIRIS is generally from 10 to 100 km and scans from 7 to 70 km tangent altitude in normal operation mode (Degenstein et al., 2009). In this study we use version v5.07 of the OSIRIS ozone data retrieved by means of the SaskMART Multiplicative Algebraic Reconstruction Technique. The retrieved profiles have a vertical resolution of approximately 2.2 km up to 40 km, degrading slightly above.

2.5 Lidars

All lidar data used in this study were provided by the NDACC community (http://www.ndacc.org, see also Steinbrecht et al., 2009a,b; McDermid et al., 1990, 1995; Brinksma et al., 2000). These lidars (at Hohenpeissenberg, Lauder, Mauna Loa, Haute Provence and Table Mountain) use the Differential Absorption Lidar (DIAL) Technique (Megie et al., 1977) to derive stratospheric ozone profiles from atmospheric measurements. Light at two different wavelengths is emitted. One wavelength is 308 nm for all lidars, while the reference wavelength is 353 nm at Hohenpeissenberg and Lauder and 355 nm for the other lidars during the investigated time period. Lidar measurements become less reliable with altitude which is reflected in deteriorating precision from approximately 1 % up to 30 km through about 2–5 % around 40 km to up to 25 % at 50 km (Nair et al., 2012). Most lidars have vertical resolutions of around 2 km for altitudes below 30 km which then increases rapidly above. More detailed information about the lidar characteristics and the measurement technique may be found in Nair et al. (2012); Megie et al. (1977). Since the recorded data are provided in terms of number density, ECMWF data were used for conversion to volume mixing ratio.

ACPD
13, 17849–17900, 2013

3 Methods

3.1 Method of trend estimation

The multilinear parametric trend model used in this study consists of a constant and a linear term, annual and semi-annual oscillation terms, as well as several harmonic overtones. The QBO was implemented using the Singapore winds at 30 hPa and 50 hPa as a proxy, which are approximately phase shifted by a quarter period and can thus be treated equivalently to sine and cosine functions of the same period length. Equation (1) is the basic function applied here, similar to Stiller et al. (2012c).

$$\hat{y}(x) = a + bx + c_1 \mathrm{qbo}_1 + d_1 \mathrm{qbo}_2 + \sum_{n=2}^{m} \left(c_n \sin\frac{2\pi x}{l_n} + d_n \cos\frac{2\pi x}{l_n}\right) \quad (1)$$

Here x is the time, whereas qbo_1 and qbo_2 refer to the Singapore winds at 30 and 50 hPa. The sum comprises 8 sine and cosine functions with the period length l_n, including the annual and semi-annual oscillation as well as 6 overtones with period lengths of 3, 4, 8, 9, 18 and 24 months. a and b represent the constant term and the slope of the fit, respectively. c_n and d_n are parameters which have to be found to fit amplitude and phase of the oscillations.

The method is based on a concept introduced by von Clarmann et al. (2010) in order to estimate trends of combined data sets which have a potential bias. By using the full covariance matrix when minimizing the cost function (cf. von Clarmann et al., 2010) an arbitrary bias can be accounted for during the regression process and thus makes the model resistant to such biases. The scheme is equivalent to fitting the trends in each data sub set individually and ignoring any jump between the subsets. The final trend then corresponds to a weighted mean of the trends of each subset. Coefficients associated with periodic and quasi-periodic variations refer to the entire data set.

In order to account for the autocorrelative nature of the atmosphere and to get realistic error estimates, the autocorrelations among the data points were considered in the

ACPD
13, 17849–17900, 2013

covariance matrix of the data set, and a model error component was assessed iteratively and added to the covariance matrix such that χ^2 of the fit approaches unity. The parameters a, b, c_n and d_n of Eq. (1) were fitted to zonal monthly means of 10° latitude bands of the MIPAS ozone time series covering 1 July 2002 to 8 April 2012 to assess the linear variation during that period. An example of the fit is shown in Fig. 1, showing the ozone monthly means as well as the fit and linear variation at 0 to 10° N and 30 km altitude. The bias between the two data blocks is quite obvious and it is reasonably accounted for during the fit process. A semi-annual oscillation and a QBO signal can also be identified in the data, which are satisfactorily reproduced by the fit.

Before analysing derived trends a potential drift in MIPAS ozone data must be identified and accounted for. To estimate the drifts against other instruments the difference of MIPAS minus the reference instrument was calculated for each data point and the related time series were fitted by the same method as just introduced. The linear term of the variation of these differences is the drift.

3.2 Drifts

In our definition, drifts are a trend-like artificial linear variation of a signal due to less than perfect instrument stability. In order to assess a clean natural trend from the measurements, possible drifts are analysed in a preceding step. This is realized by calculating the difference of the MIPAS measurement and that of another instrument at every valid altitude grid point of each coinciding profile pair, establishing monthly means of these differences and applying the trend method as introduced in Sect. 3.1. Figure 2 shows an example of the fit for the differences of Aura MLS and MIPAS. As can be seen here, there are still some oscillations in the differences, which we first expected to cancel out. When we discovered that this assumption was not justified we decided to use the full multilinear parametric regression model for drift estimation as well, including the whole set of oscillations, instead of just using a linear and a constant term. This is to account for possible dependence of the differences on the atmospheric state.

ACPD
13, 17849–17900, 2013

To improve comparability with e.g. Nair et al. (2012) we also assessed relative drifts by calculating the relative difference of each coinciding profile pair consistently with their paper as follows

$$\begin{aligned} \mathrm{vmr}_{\mathrm{rel}} &= \frac{\mathrm{vmr}_M - \mathrm{vmr}_{\mathrm{RF}}}{\mathrm{vmr}_{\mathrm{RF}}} \cdot 100\,\% \\ &= A \cdot 100\,\% \end{aligned} \tag{2}$$

The respective error was estimated accounting for Gaussian error propagation and with respect to Eq. (2).

3.2.1 Coincidence criteria

To account for varying data coverage and availability, two different coincidence criteria were used. One pair takes measurements into account which are closer than 250 km radial spatial distance and 6 h temporal difference to the MIPAS measurements. Weaker criteria of 1000 km and 24 h were applied to instruments with sparser coverage and/or fewer measurements to still obtain a sufficiently large number of measurements to compare in the drift analyses. In both cases the distance is calculated relative to the nominal geolocation of the MIPAS profile, which is the tangent point of the 30 km tangent altitude limb view. Table 2 summarizes these criteria for the different instruments and lists the total number of profiles which matched these criteria. For some instruments which originally cover the whole MIPAS mission period we additionally performed the analysis for a reduced time series, meaning that we only took coincidences of the second MIPAS period into account. This was done in order to assure that the results exhibit only minor changes when the first MIPAS period is omitted due to lack of data, e.g. for instruments like Aura MLS or ACE-FTS.

In cases with more than one measurement fulfilling the coincidence criteria, only the closest profile was chosen. This was done by normalizing the distance and time criteria as shown in Eq. (3), such that the pair with the lowest C_{comb}-value is considered to be

ACPD
13, 17849–17900, 2013

the best coincidence.

$$C_{\text{comb}} = \left(\frac{d}{d_{\text{max}}}\right)^2 + \left(\frac{t}{t_{\text{max}}}\right)^2, \quad (3)$$

where d is the spatial distance between the two profiles, d_{max} is the maximum allowed distance, t is the time difference between the profiles and t_{max} is the maximum allowed time difference. In case of two MIPAS profiles matching the same profile of the other instrument a selection process was undergone such that the loss of profiles pairs was minimized and the entirety of the pairs fulfilled the criteria best.

3.2.2 Application of the MIPAS averaging kernel

In most cases the vertical resolution of the reference instrument was better than that of MIPAS in certain altitude regions. For the lidars this region is rather the lower end of the profile, vertical resolution is certainly not better above 40 km, but as already mentioned measurements above approximately this altitude should be treated with care. The reason for applying the MIPAS averaging kernels is primarily the vertical resolution peak around 30 to 35 km in version V5R_O3_220 and V5R_O3_221 of MIPAS data from the second time period of the MIPAS mission. In the case of ACE-FTS the worst case assumption on the vertical resolution, based on the field of view, is about 3–4 km, which is very similar to that of MIPAS. Sensitivity studies showed that application of the MIPAS averaging kernels to ACE-FTS profiles does not exhibit any major differences compared to ACE-FTS profiles to which no averaging kernels were applied. However, for consistency and the afore mentioned reasons we chose to apply the respective averaging kernel of the coinciding MIPAS measurement to all instruments according to Eq. (4).

$$\tilde{\boldsymbol{x}}_{\text{fM}} = \mathbf{A}_{\text{MIPAS}}\mathbf{V}\boldsymbol{x}_{\text{f}} + (\mathbf{I} - \mathbf{A}_{\text{MIPAS}})\,\boldsymbol{x}_{\text{a}} \quad (4)$$

In this equation, $\boldsymbol{x}_{\text{f}}$ is the initially finer profile (e.g. that of Aura MLS). $\tilde{\boldsymbol{x}}_{\text{fM}}$ is that profile transferred to the MIPAS grid under consideration of the MIPAS averaging kernel

ACPD
13, 17849–17900, 2013

$\mathbf{A}_{\mathrm{MIPAS}}$. $\mathbf{V}$ is a transformation matrix relating the fine profile $\boldsymbol{x}_{\mathrm{f}}$ with the coarser grid. $\mathbf{I}$ is unity and $\boldsymbol{x}_{\mathrm{a}}$ is the a priori profile used for MIPAS. In the case of ozone a zero a priori had been used simplifying Eq. (4) to

$$\widetilde{\boldsymbol{x}}_{\mathrm{fM,O_3}} = \mathbf{A}_{\mathrm{MIPAS,O_3}} \mathbf{V} \boldsymbol{x}_{\mathrm{f,O_3}} \quad (5)$$

More detailed information on the methodology may be found in Stiller et al. (2012b).

3.3 Drift-corrected trend

Since we were interested in how the drift would influence the MIPAS ozone trend, we calculated a so-called drift-corrected trend $b_{\mathrm{corrected}}$ (Eq. 6).

$$b_{\mathrm{corrected}} = b_{\mathrm{MIPAS}} - b_{\mathrm{Drift,MIPASvsREF}} \quad (6)$$

For this purpose we used the drift estimates and calculated the difference of the MIPAS trend b_{MIPAS} and the drift versus the reference instrument $b_{\mathrm{Drift,MIPASvsREF}}$ for every altitude-latitude grid point. The associated error was simply calculated as the combined error of the MIPAS trend and the drift established in comparison versus the respective instrument, both of which were assessed within the respective regression process. Here we assume the difference to be caused by a MIPAS drift to a large extend, not by a possible drift of the other instrument. The resulting errors can be considered as a conservative estimate, because we did not account for possible correlations between the single instrument errors. If these errors were treated as positively correlated to some extent, the resulting error would decrease. Not expecting any correlation is justified here for the following reasoning: We assume that natural variability should mostly be cancelled out by calculating differences, which is the main contributor to the basic errors. Even though this is not entirely true, as shown in Sect. 3.2, this approximation is valid to a good extent, since the oscillations in the differences are considerably smaller than those in the time series of the measurements. In addition the data sets used for drift estimation are at least six times smaller than the data set used for trend estimation (MIPAS), due to only accounting for coinciding measurements.

ACPD
13, 17849–17900, 2013

4 Results

4.1 Drifts

From the drift analyses we have a wide range of results from various instruments. Comparisons with instruments which offer global or near global coverage are displayed as altitude-latitude cross-sections of the linear term of the drift analysis. Hatched areas in these plots are those where the significance of the estimated drifts is less than 2 sigma. We have performed MIPAS drift estimations versus Aura MLS, ACE-FTS and Odin OSIRIS (Figs. 3–5). Estimates versus lidars are displayed in drift panels showing the linear term of the drift analysis as well as a 2-sigma uncertainty at each altitude grid point. In the following we will focus on discussing only drifts with 2-sigma significance or better. Blue colors in Figs. 3–5 indicate that the linear variation for the MIPAS data decreases more strongly than that of the reference instrument, while red colors denote a stronger increasing linear variation for the MIPAS data.

Results for Aura MLS (Fig. 3) exhibit only negative drifts, except from very few values at lower latitudes. The negative drifts range from near zero to approximately $-0.33\,\mathrm{ppmv\,decade^{-1}}$ and seem to become slightly more negative with altitude up to $\sim 40\,\mathrm{km}$. For Odin OSIRIS (Fig. 4) we find a similar pattern, but the absolute values range down to about $-0.55\,\mathrm{ppmv\,decade^{-1}}$ at several grid points and even reach values around $-0.7\,\mathrm{ppmv\,decade^{-1}}$ in a few cases. The plots of ACE-FTS (Fig. 5) look a bit different, mainly because we found very few significant drifts overall. The remaining drifts do not seem to have a positive or negative majority in sign, so that MIPAS and ACE-FTS seem to have been measuring at similar stability during the examined time period. The large white area in the tropics, where no drifts could be calculated, results from ACE-FTS focusing on higher latitudes. Due to this there are simply not enough months during which ACE-FTS measures at low latitudes, resulting in underdetermination of the system of the multilinear parametric trend model.

Aura MLS and Odin OSIRIS do not cover the same time period. In order to assess if including the first measurement period of MIPAS makes a difference, we also analysed

ACPD
13, 17849–17900, 2013

the drifts of MIPAS versus Odin OSIRIS and two of the lidars only for the low resolution period of MIPAS (Figs. A2 and A3, respectively). It is obvious from these plots that differences compared to the drift analyses for the combined high and low spectral resolution time period of MIPAS are negligible.

Considering the lidars we assessed insignificant or negative drifts in most cases (Hohenpeissenberg, Table Mountain, Mauna Loa and Lauder). Only the comparison of MIPAS versus Observatoire Haute Provence shows positive drifts above ∼25 km, which increase with altitude and even exceed 1.0 ppmv decade^{-1} around 40 km. While the calculated drifts for the comparison of MIPAS with Mauna Loa and Lauder lidars are insignificant except for very few cases, we found significant negative drifts versus the lidar measurements at Hohenpeissenberg and Table Mountain above ∼20 km. As already observed for the analyses for MIPAS versus Aura MLS and Odin OSIRIS, these drifts seem to increase with altitude, but since the lidar data are not very reliable above 40 km it is difficult to verify maximum drift values at and above 40 km, which are apparently present in the satellite-satellite comparisons. In order to facilitate comparison with recent research (Nair et al., 2012, p. 1310) we also calculated the relative drifts of MIPAS versus these lidars as discribed in Sect. 3.2 of this paper. The results are shown in Fig. A1. We find a striking resemblance with the findings of the aforementioned authors' comparison of Aura MLS with the lidars. They also find mainly insignificant drifts for comparisons of Aura MLS with the lidar measurements of Mauna Loa and Lauder. Drifts versus lidar measurements at Hohenpeissenberg and Table Mountain are predominantly negative above ∼20 km and increase with altitude, while positive drifts dominate the results found for comparisons with measurements at Observatoire Haute Provence. Quantitatively our results are also in very good agreement with those which Nair et al. (2012) found for Aura MLS versus the lidars. Negative drifts below 40 km for MIPAS versus Hohenpeissenberg and Table Mountain measurements of down to −8.2 % decade^{-1} and −12.8 % decade^{-1} correspond to approximately −1.0 % yr^{-1} and −1.5 % yr^{-1} for Aura MLS from Nair et al. (2012), respectively. For lidar measurements at Observatoire Haute Provence positive MIPAS drifts assessed in this study range up

ACPD
13, 17849–17900, 2013

to 10 % decade^{-1} below ∼ 35 km and increase above, exceeding 15 % decade^{-1} close to 40 km, while in the comparison of Aura MLS versus the same lidar measurements Nair et al. (2012) find values smaller than 1.0 % yr^{-1} up to about 39 km and values close to 1.5 % yr^{-1} above. This indicates that the drifts are probably (at least in part) related to the lidar instruments and not the satellite instruments, e.g. Aura MLS.

There are investigations in progress concerning the calculations used to correct for the non-linearity in the MIPAS detectors during level-1b processing. Due to aging of the detectors the coefficients used for these corrections might be changing with time, instead of being constant throughout the mission, which might lead to instrumental drifts. A small set of profiles experimentally processed with recently suggested time dependent non-linearity coefficients showed more positive/less negative trends than the profiles calculated with the coefficients actually used for ESA's operational level-1 processing. Preliminary results show drifts down to maximum values of −0.3 ppmv decade^{-1} for ozone. The drifts are far smaller than −0.3 ppmv decade^{-1} at lower altitudes and seem to become slightly more negative with altitude (internal communication – cf. http://congrexprojects.com/docs/default-source/acve_docs/abstract-book-acve-for-the-web.pdf?sfvrsn=2, p. 38). So the drifts estimated regarding the old and the improved non-linearity correction coefficients indicate an ozone drift of the same sign and magnitude as those established during the drift analyses of MIPAS versus Aura MLS. This agreement between the drifts established from the comparison of MIPAS versus Aura MLS and the theoretically predicted drifts of MIPAS due to detector non-linearity suggest that it is most likely that the drifts are for the most part originated in MIPAS, not Aura MLS. In addition there has been no indication of a possible drift in the Aura MLS ozone data so far.

Due to these reasons, we believe that the assumption of an artificial drift of the order of 0 to −0.3 ppmv decade^{-1}, depending on altitude, is well justified for MIPAS ozone.

ACPD
13, 17849–17900, 2013

4.2 Amplitudes of the QBO, annual and semi-annual oscillation

Among other quantities like the drifts and trends which were assessed in this work, we took a closer look at the altitude-latitude distribution of the amplitudes of the quasi-biennial (QBO) and semi-annual oscillation (SAO) as well as of the seasonal variation of the MIPAS ozone data which were also fitted during the trend estimation process.

The amplitude of the SAO (Fig. 7) shows approximately hemispherically symmetric distributions. We find an amplitude maximum of the ozone SAO signal which is centered slightly above 30 km and exhibits maximum amplitudes of 0.5 ppmv. Beyond tropical latitudes the amplitude decreases rapidly to near zero values, except in the polar region. These findings agree very well with the results of Huang et al. (2008), who analysed QBO and SAO ozone signals based on the Sounding of the Atmosphere using Broadband Emission Radiometry (SABER) satellite measurements for 2002 through 2005 from 20 to 100 km and for latitudes within 48° N and S, and found good agreement with ozone data of the Microwave Limb Sounder on the Upper Atmosphere Research Satellite (UARS MLS). They assess an amplitude maximum of ∼ 0.5 ppmv between 30 and 35 km for ozone, which is a result remarkably similar to ours.

The amplitude of the ozone QBO signal A_{QBO} is calculated as in Eq. (7) (cf. Eq. 1).

$$A_{\mathrm{QBO}} = \frac{d_1}{\sin\left(\arctan\left(\frac{d_1}{c_1}\right)\right)} \tag{7}$$

Its distribution, which is displayed in Fig. 8, shows a slightly more complex structure. Beside two tropical maxima around 25 km, with slightly over 0.6 ppmv, and 35 km, with approximately 0.4 ppmv, we find two additional subtropical maxima slightly above 30 km on both hemispheres. Of the latter two areas, the Northern Hemisphere one shows larger amplitudes with values of nearly 0.6 ppmv, while the Southern Hemisphere area is spatially larger but exhibits smaller maximum values of more than 0.3 ppmv for severaly grid points but none reaching 0.4 ppmv.

ACPD
13, 17849–17900, 2013

The location of these maxima in the QBO ozone amplitude agrees very well with previous findings of e.g. Zawodny and McCormick (1991) who find tropical maxima in SAGE II data located between 20–27 km and 30–38 km, Randel and Wu (1996), who report extra-tropical maxima located close to 30 km in latitude ranges of 10–60° also from SAGE II data, as well as Fadnavis and Beig (2009) who find tropical maxima around 22 hPa (∼ 26 km) and 9 hPa (∼ 32 km) at equatorial latitudes and weaker extra-tropical maxima. The values of the reported maxima are larger though (about 1 ppmv (Randel et al., 1999) to 1.4–1.6 ppmv (Fadnavis and Beig, 2009)), showing the larger values at the higher tropical maximum. MIPAS amplitudes are smaller, which might partly be due to the coarse vertical resolution especially around the upper maximum in tropical latitudes. The pattern could be understood as a periodic expansion and shrinking of the ozone maximum in the tropics with the QBO phase both in vertical and meridional direction. In this case, the amplitudes would be largest where the ozone gradient in both vertical and meridional direction is largest, which is what we observe (cf. Fig. 12, which is discussed in detail in Sect. 4.3).

We chose to show the seasonal variation in terms of relative values, because otherwise the important regions for this variation, along the tropopause, fade into the background since the absolute ozone values are much smaller in these regions than above. In the Tropical Tropopause Layer (TTL) vertical motion has a great impact on the ozone amplitude, while at higher latitudes meridional mixing plays an important role. Around the tropical tropopause (16–18 km; ∼ 20° S to ∼ 20° N) an area of strong seasonal variation is visible. Most values of the absolute amplitude in this region are within ∼ 0.01 and ∼ 0.06 ppmv with few outliers reaching up to ∼ 0.11 ppmv. In the extratropical Upper Troposphere Lower Stratosphere (UTLS: 10–22 km; 40–60° S/N) the signal of the ozone variation is clearly visible around the tropopause and below. The values of the ozone amplitude in this region range from ∼ 0.1 to ∼ 0.8 ppmv in the Northern Hemisphere and from ∼ 0.01 to ∼ 0.6 ppmv in the Southern Hemisphere. We also see a signal in polar regions reaching up beyond 40 km with absolute values of up to 1.23 ppmv in the Northern Hemisphere. In the Southern Hemisphere around 30 km we

ACPD
13, 17849–17900, 2013

find AO amplitude of ∼1.0 ppmv and ∼1.24 ppmv between 40 km and 50 km. These results were found to be in very good agreement with recent findings. Eyring et al. (2010) report amplitudes of ∼0.05 ppmv for NIWA observations between 20° S–20° N at 100 hPa (∼16 km), while some models show amplitudes ranging up to ∼0.1 ppmv. For the extratropical UTLS region in the Northern Hemisphere, ozone AO amplitudes of ∼0.5 ppmv were deduced from Aura MLS and a multimodel mean at 100 hPa, while at 200 hPa (∼12 km) ∼0.3 ppmv were found for the ozone AO amplitude in Aura MLS and a slightly smaller amplitude of ∼0.2 ppmv was assessed from the multimodel mean. For the Southern Hemisphere amplitudes of ∼0.4 ppmv and ∼0.1 ppmv were found at pressure levels of 100 hPa and 200 hPa, respectively. These amplitudes are very similar to those we found in the MIPAS ozone data. Tegtmeier et al. (2013) report ozone AO amplitudes of ∼0.15 ppmv for a multi-instrument mean at 80 hPa (∼17 km) between 20° N and S for the period of 2005 to 2010. For southern mid-latitudinal regions (40–50° S) an amplitude of ∼0.15 ppmv was deduced from the multi-instrument mean at 200 hPa for the same time period as mentioned above. In the Northern Hemisphere at 50 hPa the multi-instrument mean shows an amplitude of ∼1.2 ppmv. Some of these amplitudes are larger than those deduced from MIPAS ozone data during this analyses. However, Tegtmeier et al. (2013) offer the explanation, that this might be due to significantly better vertical resolution of some of the instruments used in their analysis.

4.3 Linear variations (short term trends)

The linear term of the analysis of the MIPAS data estimated with the method described in Sect. 3.1 represents a short term trend of the evolution of stratospheric ozone during the past 10 yr. Similar as for the drifts, we will concentrate on 2-sigma significant trends throughout the following discussion. As can be seen in Fig. 10, this excludes most of the results beyond 60° N and S, where natural variability is large and thus the simple multilinear parametric trend model can presumably not fit the data properly. However, we should keep in mind that the non-random pattern of the estimated trends is a strong hint that increased significance could be achieved by a reduced spatial resolution of

ACPD
13, 17849–17900, 2013

the analysis, both in the vertical and the latitudinal domain. Most of the trends below 20 km are non-significant, probably because ozone values are very small and MIPAS measurements are inhibited by clouds especially at low latitudes.

The results of this part of the trend analysis are displayed in Fig. 10 by means of an altitude-latitude cross-section and show a northern-southern hemispherically asymmetric pattern. We found a larger number of 2 sigma-significant trends for Southern Hemisphere latitudes in general. In addition these significant trends exhibit predominantly positive values. A pronounced positive area ranges from the subtropics to near polar latitudes centered approximately around 30 km and with maximum ozone trend values of +0.5 ppmv decade^{-1}. Apart from that we find a few smaller areas which also exhibit weaker positive trends, e.g. in the tropics around 20 km, at northern subtropical latitudes slightly above 30 km, at northern mid latitudes at approximately 45 km and at subtropical latitudes below 20 km in both hemispheres. Negative trends are observed in the tropics in the form of a double peak structure with maxima at approximately 25 and 35 km which reveal minimum trends of −0.5 ppmv decade^{-1}. Considerably smaller values appear at Northern Hemisphere mid latitudes between 20 and 30 km.

Negative ozone trends in the tropical middle stratosphere have also been found in SCIAMACHY data (Gebhardt et al., 2013). Generally the trends shown in their paper agree with ours, but not in every detail. In particular the trends provided by Gebhardt et al. (2013) for the middle tropics are more negative with only one negative peak.

Kyrölä et al. (2013) see less negative trends in the tropics around 30 to 35 km than Gebhardt et al. (2013). The trends by Kyrölä et al. (2013) are of the order of −2 to −3 % decade^{-1}. This is even a bit smaller than what we find, but in their paper the time period looked at (1997–2011) is a bit longer than ours and covers a slightly different time span in general. Thus differences can be expected when comparing their results with ours. In the extratropics up to ∼ 50° N/S Kyrölä et al. (2013) find predominantly positive or near zero trends between 25 and 50 km. Their trends are in the order of up to +2 % decade^{-1} in these regions. This agrees considerably well with our results. Comparing our results with others of the post mid 1990s period we find that the

ACPD
13, 17849–17900, 2013

assessed changes are predominantly positive or near zero, except for the lower stratospheric tropics. While column ozone from ground-based and satellite measurements seem to exhibit non-changing ozone values in the mid-latitudes for both hemispheres after 1998 after showing an increase of ∼2 % from 1996 to 1998, an increase in mid-latitudinal ozone was found for the Northern Hemisphere for the time period of 1996 to 2009 at altitude ranges of 12–15, 20–25 and 35–45 km with largest increases (6 %) at the lowest level and smaller values above. Southern Hemisphere mid latitudinal trends were only found to be statistically significant at the highest level (35–45 km) exhibiting an increase of 1–3 % for the time period of 1996 to 2009 (cf. WMO, 2011, Chapter 2, Table S2-1). Tropical ozone trends from simulations show negative values right above the tropopause (18–19 km), presumably due to increased upwelling.

In addition to the trends estimated from MIPAS measurements, we also calculated "drift-corrected trends" (Fig. 11). The displayed trends and associated errors were calculated as described in Sect. 3.3. We chose the drift estimates versus Aura MLS for correction of the MIPAS trends due to two reasons. First, a drift of the order of magnitude such as the one established by comparison with Aura MLS can mostly be explained by drifts associated with the non-linearity correction for the MIPAS detector as already mentioned in Sect. 4.1. Second, there has been no indication of a possible drift in Aura MLS ozone data so far. In addition to that the number of coinciding profiles with Aura MLS is the largest compared to all other instruments, even when using strict coincidence criteria, which presumably provides the most reliable analysis. Thus the drift estimate versus Aura MLS seems to be the most suitable candidate for shifting the MIPAS trends towards reality. While one might think that the drift-corrected MIPAS trends using Aura MLS for drift determination gives actually an Aura MLS ozone trend, this is not true: The MIPAS trend is inferred from a by far larger data set than that used for drift estimation. For the drift estimation of MIPAS-Aura MLS coincidences had to be used, while the trends have been inferred from the entire MIPAS data set. Most of the negative ozone trends which were significant in the pure MIPAS estimates are no longer significant at 2-sigma level in the corrected version, especially at higher

ACPD
13, 17849–17900, 2013

altitudes. In addition, significant areas with positive trends become larger and more significant. These results agree better with recent findings (e.g. WMO, 2011; Steinbrecht et al., 2009a) than the MIPAS trends without any correction. The few negative trends left are the tropical double peak structure and Northern Hemisphere areas around 20 to 25 km, as well as a very small spot around 45 km. A clear hemispherically asymmetric distribution is still visible. Positive values reach up to +0.55 ppmv decade^{-1} in the Southern Hemisphere and +0.46 ppmv decade^{-1} in the Northern Hemisphere, with the northern hemispheric areas slightly above 40 km now reaching values of maximum +0.40 ppmv decade^{-1}. The tropical negative peaks come up with minimum values of −0.37 ppmv decade^{-1} and −0.41 ppmv decade^{-1} for the lower and the upper one, respectively.

A reasonable explanation for negative trends near the equator is increased tropical upwelling, as suggested before (WMO, 2011), but only for altitudes slightly above the tropopause. So upwelling does not provide a sufficient explanation for the negative values in the tropical middle stratosphere. It cannot explain the double peak structure either. The altitude-latitude cross-section of the amplitude of the QBO shows that the negative peaks in the trends coincide closely with the maxima in QBO amplitude. While the pattern of the QBO amplitude hints towards a periodic expansion and shrinking of the ozone maximum in the tropics (see Sect. 4.2), the trend pattern hints towards a vertical shrinking and meridional expansion of the ozone maximum. This is also most pronounced where the gradient in the ozone distribution is largest. According to this it is reasonable for the maxima of the QBO amplitude and the extrema of the trends to occur in similar areas. Figures 12 and 13 show the zonal ozone distribution calculated from the results of the parametric trend fit for the years 2000 and 2012, respectively. While the constant term for the year 2000 is a direct output of the trend fit process, the constant term for the year 2012 was calculated by extrapolating the ozone volume mixing ratio from the year 2000 to the year 2012 using the drift-corrected trend which was assessed previously. One can see a vertical shrinking and latitudinal expansion of the ozone maximum in the tropics.

ACPD
13, 17849–17900, 2013

The hemispherically asymmetric trend patterns shown in Fig. 11 could be explained by a shift of the subtropical mixing barriers by 5° to the south over the observation period, as first indicated by Stiller et al. (2012a). A simple way to mimic this shift is shown in Fig. 14: the zonal mean distribution of ozone as obtained from the constant terms of the parametric fits of the time series for all latitude-altitude bins has been shifted by 5° to the south below altitudes of 30 km. Above 30 km, the Northern Hemisphere (20° to 60° N) has been shifted to the North, simulating a widening of the tropical pipe. The shifts have been applied between 60° S and 60° N only, since a shift to the polar mixing barriers was not expected. The differences between the original and the shifted distribution assumed to appear over a period of 10 yr is shown in Fig. 14. The pattern of the change of the ozone distribution over a decade is stunningly similar to the linear trends observed in the real ozone distributions. Since the main features of the zonal ozone distribution are to a large extent ruled by the subtropical mixing barriers a shift of the barriers by 5° to the south (and an expansion of the tropical pipe above 30 km) would be able to explain the observed decadal linear trend to a large degree. We do not claim however, that this is a climatological trend, but possibly rather a low-frequency natural variability, the causes of which are still unknown.

5 Conclusions

The investigations performed in this work offer an overall coherent picture. We calculated drifts of the MIPAS ozone time series versus several instruments which include satellite as well as ground based experiments. Most of these analyses suggest that MIPAS ozone data most probably has a small negative drift and thus trends calculated from the MIPAS data might exhibit values which are less positive (more negative) than in reality. Only few comparisons suggest that MIPAS ozone data do not reveal a drift, such as the drift estimation versus ACE-FTS, or even hint at positive drifts like the analysis comparing MIPAS with the Lidar at Observatoire Haute Provence. Magnitudes of the established negative drifts differ from minimum values

ACPD
13, 17849–17900, 2013

of about $-0.3\,\mathrm{ppmv\,decade^{-1}}$ for Aura MLS to approximately $-0.7\,\mathrm{ppmv\,decade^{-1}}$ for Odin OSIRIS and for some lidars at high altitudes. Due to recent studies on MIPAS' non linearity correction and the analysis versus Aura MLS, which presumably offers the most reliable drift estimates, we assume that a drift in MIPAS ozone data is most likely of a magnitude of 0 to $-0.3\,\mathrm{ppmv\,decade^{-1}}$, depending on latitude, and thus we correct our trends estimated from MIPAS data by the drift estimates of the comparison with Aura MLS. The corrected trends agree well with recent findings and offer better agreement with those findings than the non-corrected trends. They range from approximately $-0.4\,\mathrm{ppmv\,decade^{-1}}$ in the tropics up to $+0.55\,\mathrm{ppmv\,decade^{-1}}$ at southern mid-latitudes. Significant areas exhibiting positive values increase spatially when correcting with the drift estimated in comparison with Aura MLS, leaving mostly positive values. This is in very good agreement with results shown in WMO (2011). In the aforementioned work there are predominantly positive or close to zero trends found for the period after 1996/1997.

We observe a negative double peak structure around the equator, with minima at approximately 25 and 35 km, exhibiting extreme values of $-0.37\,\mathrm{ppmv\,decade^{-1}}$ and $-0.41\,\mathrm{ppmv\,decade^{-1}}$ respectively, which coincide in altitude with the maxima of the amplitude of the ozone QBO. This coincidence of the tropical QBO maxima with the negative ozone trends occurs due to the ozone gradient being largest at these altitudes, so that the periodic vertical expansion and shrinking (in case of the QBO) and the vertical flattening of the ozone maximum over the measured period (in case of the trends) both are very obvious here. We find a clear hemispherically asymmetric pattern in the trends with the negative signs in the northern lower stratosphere and positive values in the southern lower stratosphere (20–30 km). This, together with negative trends at tropical mid-stratospheric altitudes can be mimicked by shifting the zonal ozone distribution 30 km by 5° to the South and expanding the tropical pipe by 5° to the North and South above, simulating mainly a respective shift of the subtropical mixing barriers over the observation period. Even the positive trends just above the tropical tropopause can be simulated by the shift of the subtropical mixing barriers to the South. Such a shift

ACPD
13, 17849–17900, 2013

is not necessarily a climatological trend, but possibly rather a low-frequency natural variation, the cause of which is still unknown.

The altitude-latitude cross-sections of the amplitudes of the QBO, SAO and the seasonal variation agree well with previous results. In case of the SAO, both the altitude-latitude distribution as well as the magnitude are very similar to previous findings, while the estimated values of the ozone QBO amplitude are smaller than those found in other studies. Our results for the amplitudes of the seasonal variation show reasonable altitude-latitude distributions and reveal similar magnitudes as previous findings.

The service charges for this open access publication have been covered by a Research Centre of the Helmholtz Association.

Acknowledgements. The retrievals of IMK/IAA were partly performed on the HP XC4000 of the Scientific Supercomputing Center (SSC) Karlsruhe under project grant MIPAS. IMK data analysis was supported by DLR under contract number 50EE0901. MIPAS level 1B data were provided by ESA. We acknowledge support by Deutsche Forschungsgemeinschaft and Open Access Publishing Fund of Karlsruhe Institute of Technology. The Atmospheric Chemistry Experiment (ACE), also known as SCISAT, is a Canadian-led mission mainly supported by the Canadian Space Agency and the Natural Sciences and Engineering Research Council of Canada. Work at the Jet Propulsion Laboratory, California Institute of Technology, was carried out under contract with the National Aeronautics and Space Administration.

References

Brinksma, E. J., Bergwerff, J. B., Bodeker, G. E., Boersma, K. F., Boyd, I. S., Connor, B. J., de Haan, J. F., Hogervorst, W., Hovenier, J. W., Parrish, A., Tsou, J. J., Zawodny, J. M., and Swart, D. P. J.: Validation of 3 years of ozone measurements over Network for the Detection of Stratospheric Change station Lauder, New Zealand, J. Geophys. Res., 105, 17291, doi:10.1029/2000JD900143, 2000. 17858

ACPD
13, 17849–17900, 2013

Degenstein, D. A., Bourassa, A. E., Roth, C. Z., and Llewellyn, E. J.: Limb scatter ozone retrieval from 10 to 60 km using a multiplicative algebraic reconstruction technique, Atmos. Chem. Phys., 9, 6521–6529, doi:10.5194/acp-9-6521-2009, 2009. 17857, 17858

Dobson, G. M. B.: Ozone in the upper atmosphere and its relation to meteorology, Nature, 127, 668–672, doi:10.1038/127668a0, 1931. 17852

Dobson, G. M. B.: Forty years' research on atmospheric ozone at Oxford: a history, Appl. Optics, 7, 387, doi:10.1364/AO.7.000387, 1968. 17852

Dupuy, E., Walker, K. A., Kar, J., Boone, C. D., McElroy, C. T., Bernath, P. F., Drummond, J. R., Skelton, R., McLeod, S. D., Hughes, R. C., Nowlan, C. R., Dufour, D. G., Zou, J., Nichitiu, F., Strong, K., Baron, P., Bevilacqua, R. M., Blumenstock, T., Bodeker, G. E., Borsdorff, T., Bourassa, A. E., Bovensmann, H., Boyd, I. S., Bracher, A., Brogniez, C., Burrows, J. P., Catoire, V., Ceccherini, S., Chabrillat, S., Christensen, T., Coffey, M. T., Cortesi, U., Davies, J., De Clercq, C., Degenstein, D. A., De Mazière, M., Demoulin, P., Dodion, J., Firanski, B., Fischer, H., Forbes, G., Froidevaux, L., Fussen, D., Gerard, P., Godin-Beekmann, S., Goutail, F., Granville, J., Griffith, D., Haley, C. S., Hannigan, J. W., Höpfner, M., Jin, J. J., Jones, A., Jones, N. B., Jucks, K., Kagawa, A., Kasai, Y., Kerzenmacher, T. E., Kleinböhl, A., Klekociuk, A. R., Kramer, I., Küllmann, H., Kuttippurath, J., Kyrölä, E., Lambert, J.-C., Livesey, N. J., Llewellyn, E. J., Lloyd, N. D., Mahieu, E., Manney, G. L., Marshall, B. T., McConnell, J. C., McCormick, M. P., McDermid, I. S., McHugh, M., McLinden, C. A., Mellqvist, J., Mizutani, K., Murayama, Y., Murtagh, D. P., Oelhaf, H., Parrish, A., Petelina, S. V., Piccolo, C., Pommereau, J.-P., Randall, C. E., Robert, C., Roth, C., Schneider, M., Senten, C., Steck, T., Strandberg, A., Strawbridge, K. B., Sussmann, R., Swart, D. P. J., Tarasick, D. W., Taylor, J. R., Tétard, C., Thomason, L. W., Thompson, A. M., Tully, M. B., Urban, J., Vanhellemont, F., Vigouroux, C., von Clarmann, T., von der Gathen, P., von Savigny, C., Waters, J. W., Witte, J. C., Wolff, M., and Zawodny, J. M.: Validation of ozone measurements from the Atmospheric Chemistry Experiment (ACE), Atmos. Chem. Phys., 9, 287–343, doi:10.5194/acp-9-287-2009, 2009. 17857

Eyring, V., Shepherd, T. G., and Waugh, D. W. (Eds.): SPARC Report on the Evaluation of Chemistry-Climate Models, SPARC Report No.5, WCRP-132, WMO/TD-No. 1526, SPARC CCMVal, 2010. 17869

Fadnavis, S. and Beig, G.: Quasi-biennial oscillation in ozone and temperature over tropics, J. Atmos. Sol.-Terr. Phy., 71, 257–263, doi:10.1016/j.jastp.2008.11.012, 2009. 17868

ACPD
13, 17849–17900, 2013

Farman, J. C., Gardiner, B. G., and Shanklin, J. D.: Large losses of total ozone in Antarctica reveal seasonal ClO_x/NO_x interaction, Nature, 315, 207–210, doi:10.1038/315207a0, 1985. 17852

Fischer, H., Birk, M., Blom, C., Carli, B., Carlotti, M., von Clarmann, T., Delbouille, L., Dudhia, A., Ehhalt, D., Endemann, M., Flaud, J. M., Gessner, R., Kleinert, A., Koopman, R., Langen, J., López-Puertas, M., Mosner, P., Nett, H., Oelhaf, H., Perron, G., Remedios, J., Ridolfi, M., Stiller, G., and Zander, R.: MIPAS: an instrument for atmospheric and climate research, Atmos. Chem. Phys., 8, 2151–2188, doi:10.5194/acp-8-2151-2008, 2008. 17854

Froidevaux, L., Jiang, Y. B., Lambert, A., Livesey, N. J., Read, W. G., Waters, J. W., Browell, E. V., Hair, J. W., Avery, M. A., McGee, T. J., Twigg, L. W., Sumnicht, G. K., Jucks, K. W., Margitan, J. J., Sen, B., Stachnik, R. A., Toon, G. C., Bernath, P. F., Boone, C. D., Walker, K. A., Filipiak, M. J., Harwood, R. S., Fuller, R. A., Manney, G. L., Schwartz, M. J., Daffer, W. H., Drouin, B. J., Cofield, R. E., Cuddy, D. T., Jarnot, R. F., Knosp, B. W., Perun, V. S., Snyder, W. V., Stek, P. C., Thurstans, R. P., and Wagner, P. A.: Validation of Aura Microwave Limb Sounder stratospheric ozone measurements, J. Geophys. Res.-Atmos., 113, D15S20, doi:10.1029/2007JD008771, 2008. 17856

Gebhardt, C., Rozanov, A., Hommel, R., Weber, M., Bovensmann, H., Burrows, J. P., Degenstein, D., Froidevaux, L., and Thompson, A. M.: Stratospheric ozone trends and variability as seen by SCIAMACHY during the last decade, Atmos. Chem. Phys. Discuss., 13, 11269–11313, doi:10.5194/acpd-13-11269-2013, 2013. 17870

Glatthor, N., von Clarmann, T., Fischer, H., Funke, B., Gil-López, S., Grabowski, U., Höpfner, M., Kellmann, S., Linden, A., López-Puertas, M., Mengistu Tsidu, G., Milz, M., Steck, T., Stiller, G. P., and Wang, D.-Y.: Retrieval of stratospheric ozone profiles from MIPAS/ENVISAT limb emission spectra: a sensitivity study, Atmos. Chem. Phys., 6, 2767–2781, doi:10.5194/acp-6-2767-2006, 2006. 17854, 17855

Götz, F. W. P., Meetham, A. R., and Dobson, G. M. B.: The Vertical Distribution of Ozone in the Atmosphere, P. R. Soc. A, 145, 416–446, doi:10.1098/rspa.1934.0109, 1934. 17852

Huang, F. T., Mayr, H. G., Reber, C. A., Russell III, J. M., Mlynczak, M. G., and Mengel, J. G.: Ozone quasi-biennial oscillations (QBO), semiannual oscillations (SAO), and correlations with temperature in the mesosphere, lower thermosphere, and stratosphere, based on measurements from SABER on TIMED and MLS on UARS, J. Geophys. Res., 113, A01316, doi:10.1029/2007JA012634, 2008. 17867

ACPD
13, 17849–17900, 2013

Kyrölä, E., Laine, M., Sofieva, V., Tamminen, J., Päivärinta, S.-M., Tukiainen, S., Zawodny, J., and Thomason, L.: Combined SAGE II-GOMOS ozone profile data set 1984–2011 and trend analysis of the vertical distribution of ozone, Atmos. Chem. Phys. Discuss., 13, 10661–10700, doi:10.5194/acpd-13-10661-2013, 2013. 17870

Laeng, L., Grabowski, U., von Clarmann, T., Stiller, G., Kellmann, S., Kiefer, M., Linden, A., Lossow, S., Bathgate, T., Bernath, P., Boone, C. D., Clerbaux, C., Degenstein, D., and Fritz, S., Froidevaux, L., Hervig, M., Hoppel, K., Lumpe, J., McHugh, M., Sano, T., Sofieva, V., Suzuki, M., Tamminen, J., Urban, J., Walker, K., Weber, M., and Zawodny, J.: Validation of MIPAS IMK/IAA ozone profiles, Poster at Quadrennial Ozone Symposium 2012, Toronto, 27–31 August, 2012. 17855

Llewellyn, E., Lloyd, N. D., Degenstein, D. A., Gattinger, R. L., Petelina, S. V., Bourassa, A. E., Wiensz, J. T., Ivanov, E. V., McDade, I. C., Solheim, B. H., McConnell, J. C., Haley, C. S., von Savigny, C., Sioris, C. E., McLinden, C. A., Griffioen, E., Kaminski, J., Evans, W. F. J., Puckrin, E., Strong, K., Wehrle, V., Hum, R. H., Kendall, D. J. W., Matsushita, J., Murtagh, D. P., Brohede, S., Stegman, J., Witt, G., Barnes, G., Payne, W. F., Piche, L., Smith, K., Warshaw, G., Deslauniers, D. L., Marchand, P., Richardson, E. H., King, R. A., Wevers, I., McCreath, W., Kyrola, E., Oikarinen, L., Leppelmeier, G. W., Auvinen, H., Megie, G., Hauchecorne, A., Lefevre, F., de La Noe, J., Ricaud, P., Frisk, U., Sjoberg, F., von Scheele, F., and Nordh, L.: The OSIRIS instrument on the Odin spacecraft, Can. J. Phys., 82, 411–422, doi:10.1139/p04-005, 2004. 17858

McDermid, I. S., Walsh, T. D., Deslis, A., and White, M. L.: Optical systems design for a stratospheric lidar system, Appl. Optics, 34, 6201, doi:10.1364/AO.34.006201, 1995. 17858

McDermid, S. I., Godin, S. M., and Lindqvist, L. O.: Ground-based laser DIAL system for long-term measurements of stratospheric ozone, Appl. Optics, 29, 3603–3612, doi:10.1364/AO.29.003603, 1990. 17858

Megie, G., Allain, J. Y., Chanin, M. L., and Blamont, J. E.: Vertical profile of stratospheric ozone by lidar sounding from the ground, Nature, 270, 329–331, doi:10.1038/270329a0, 1977. 17858

Molina, M. J. and Rowland, F. S.: Stratospheric sink for chlorofluoromethanes: chlorine atom–catalysed destruction of ozone, Nature, 249, 810–812, 1974. 17852

Nair, P. J., Godin-Beekmann, S., Froidevaux, L., Flynn, L. E., Zawodny, J. M., Russell III, J. M., Pazmiño, A., Ancellet, G., Steinbrecht, W., Claude, H., Leblanc, T., McDermid, S., van Gijsel, J. A. E., Johnson, B., Thomas, A., Hubert, D., Lambert, J.-C., Nakane, H., and

ACPD
13, 17849–17900, 2013

Swart, D. P. J.: Relative drifts and stability of satellite and ground-based stratospheric ozone profiles at NDACC lidar stations, Atmos. Meas. Tech., 5, 1301–1318, doi:10.5194/amt-5-1301-2012, 2012. 17858, 17861, 17865, 17866

Randel, W. J. and Wu, F.: Isolation of the ozone QBO in SAGE II data by singular-value decomposition, J. Atmos. Sci., 53, 2546–2560, doi:10.1175/1520-0469(1996)053<2546:IOTOQI>2.0.CO;2, 1996. 17868

Randel, W. J., Wu, F., Swinbank, R., Nash, J., and O'Neill, A.: Global QBO circulation derived from UKMO stratospheric analyses, J. Atmos. Sci., 56, 457–474, doi:10.1175/1520-0469(1999)056<0457:GQCDFU>2.0.CO;2, 1999. 17868

Schoeberl, M. R., Douglass, A. R., Hilsenrath, E., Bhartia, P. K., Beer, R., Waters, J. W., Gunson, M. R., Froidevaux, L., Gille, J. C., Barnett, J. J., Levelt, P. F., and de Cola, P.: Overview of the EOS aura mission, IEEE T. Geosci. Remote, 44, 1066–1074, doi:10.1109/TGRS.2005.861950, 2006. 17856

Steck, T., von Clarmann, T., Fischer, H., Funke, B., Glatthor, N., Grabowski, U., Höpfner, M., Kellmann, S., Kiefer, M., Linden, A., Milz, M., Stiller, G. P., Wang, D. Y., Allaart, M., Blumenstock, Th., von der Gathen, P., Hansen, G., Hase, F., Hochschild, G., Kopp, G., Kyrö, E., Oelhaf, H., Raffalski, U., Redondas Marrero, A., Remsberg, E., Russell III, J., Stebel, K., Steinbrecht, W., Wetzel, G., Yela, M., and Zhang, G.: Bias determination and precision validation of ozone profiles from MIPAS-Envisat retrieved with the IMK-IAA processor, Atmos. Chem. Phys., 7, 3639–3662, doi:10.5194/acp-7-3639-2007, 2007. 17855

Steinbrecht, W., Claude, H., Schonenborn, F., McDermid, I. S., Leblanc, T., Godin-Beekmann, S., Keckhut, P., Hauchecorne, A., van Gijsel, J. A. E., Swart, D. P. J., Bodeker, G. E., Parrish, A., Boyd, I. S., Kampfer, N., Hocke, K., Stolarski, R. S., Frith, S. M., Thomason, L. W., Remsberg, E. E., von Savigny, C., Rozanov, A., and Burrows, J. P.: Ozone and temperature trends in the upper stratosphere at five stations of the Network for the Detection of Atmospheric Composition Change, Int. J. Remote Sens., 30, 3875–3886, doi:10.1080/01431160902821841, 2009a. 17853, 17858, 17872

Steinbrecht, W., McGee, T. J., Twigg, L. W., Claude, H., Schönenborn, F., Sumnicht, G. K., and Silbert, D.: Intercomparison of stratospheric ozone and temperature profiles during the October 2005 Hohenpeißenberg Ozone Profiling Experiment (HOPE), Atmos. Meas. Tech., 2, 125–145, doi:10.5194/amt-2-125-2009, 2009b. 17858

Stiller, G., Von Clarmann, T., Eckert, E., Haenel, F., Funke, B., Glatthor, N., Grabowski, U., Kellmann, S., Kiefer, M., Linden, A., Lossow, S., and López-Puertas, M.: Global observa-

ACPD
13, 17849–17900, 2013

tion of stratospheric age of air, its temporal variation, and correlation with ozone, Poster at Quadrennial Ozone Symposium 2012, Toronto, 27–31 August, 2012a. 17873

Stiller, G. P., Kiefer, M., Eckert, E., von Clarmann, T., Kellmann, S., García-Comas, M., Funke, B., Leblanc, T., Fetzer, E., Froidevaux, L., Gomez, M., Hall, E., Hurst, D., Jordan, A., Kämpfer, N., Lambert, A., McDermid, I. S., McGee, T., Miloshevich, L., Nedoluha, G., Read, W., Schneider, M., Schwartz, M., Straub, C., Toon, G., Twigg, L. W., Walker, K., and Whiteman, D. N.: Validation of MIPAS IMK/IAA temperature, water vapor, and ozone profiles with MOHAVE-2009 campaign measurements, Atmos. Meas. Tech., 5, 289–320, doi:10.5194/amt-5-289-2012, 2012b. 17855, 17863

Stiller, G. P., von Clarmann, T., Haenel, F., Funke, B., Glatthor, N., Grabowski, U., Kellmann, S., Kiefer, M., Linden, A., Lossow, S., and López-Puertas, M.: Observed temporal evolution of global mean age of stratospheric air for the 2002 to 2010 period, Atmos. Chem. Phys., 12, 3311–3331, doi:10.5194/acp-12-3311-2012, 2012c. 17859

Tegtmeier, S., Hegglin, M. I., Anderson, J., Bourassa, A., and Brohede, S., Degenstein, D., Froidevaux, L., Fuller, L., Funke, B., Gille, J., Jones, A., Kasai, Y., Kyrölä, E., Lingenfelser, G., Lumpe, J., Nardi, B., Neu, J., Pendlebury, D., Remsberg, E., Rozanov, A., Smith, L., Toohey, M., Urban, J., von Clarmann, T., Walker, K., and Wang, R.: The SPARC data initiative: a comparison of ozone climatologies from international limb satellite sounders, submitted, J. Geophys. Res., 2013. 17869

von Clarmann, T., Höpfner, M., Kellmann, S., Linden, A., Chauhan, S., Funke, B., Grabowski, U., Glatthor, N., Kiefer, M., Schieferdecker, T., Stiller, G. P., and Versick, S.: Retrieval of temperature, H_2O, O_3, HNO_3, CH_4, N_2O, $ClONO_2$ and ClO from MIPAS reduced resolution nominal mode limb emission measurements, Atmos. Meas. Tech., 2, 159–175, doi:10.5194/amt-2-159-2009, 2009. 17855

von Clarmann, T., Stiller, G., Grabowski, U., Eckert, E., and Orphal, J.: Technical Note: Trend estimation from irregularly sampled, correlated data, Atmos. Chem. Phys., 10, 6737–6747, doi:10.5194/acp-10-6737-2010, 2010. 17859

Waters, J. W., Froidevaux, L., Harwood, R. S., Jarnot, R. F., Pickett, H. M., Read, W. G., Siegel, P. H., Cofield, R. E., Filipiak, M. J., Flower, D. A., Holden, J. R., Lau, G. K., Livesey, N. J., Manney, G. L., Pumphrey, H. C., Santee, M. L., Wu, D. L., Cuddy, D. T., Lay, R. R., Loo, M. S., Perun, V. S., Schwartz, M. J., Stek, P. C., Thurstans, R. P., Boyles, M. A., Chandra, K. M., Chavez, M. C., Chen, G.-S., Chudasama, B. V., Dodge, R., Fuller, R. A., Girard, M. A., Jiang, J. H., Jiang, Y., Knosp, B. W., Labelle, R. C., Lam, J. C.,

ACPD
13, 17849–17900, 2013

Lee, A. K., Miller, D., Oswald, J. E., Patel, N. C., Pukala, D. M., Quintero, O., Scaff, D. M., Vansnyder, W., Tope, M. C., Wagner, P. A., and Walch, M. J.: The Earth Observing System Microwave Limb Sounder (EOS MLS) on the Aura Satellite, IEEE T. Geosci. Remote, 44, 1075–1092, doi:10.1109/TGRS.2006.873771, 2006. 17856

WMO: Scientific Assessment of Ozone Depletion: 2010, Global Ozone Research and Monitoring Project 52, World Meteorological Organisation, Geneva, Switzerland, 516 pp., 2011. 17853, 17871, 17872, 17874

Zawodny, J. M. and McCormick, M. P.: Stratospheric Aerosol and Gas Experiment II measurements of the quasi-biennial oscillations in ozone and nitrogen dioxide, J. Geophys. Res., 96, 9371–9377, doi:10.1029/91JD00517, 1991. 17868

ACPD
13, 17849–17900, 2013

Table 1. Overview of the instruments, important characteristics and time spans used for the drift analyses.

Instrument	Version	Vertical resolution	Period used for analyses
MIPAS Envisat	V3O_O3_9	~ 3.5–5 km up to 40 km; slowly degrading above	Jul 2002–Mar 2004
MIPAS Envisat	V5R_O3_220 & V5R_O3_221	~ 2.5–5 km; largest values around ~ 30–35 km	Jan 2005–Apr 2012
ACE-FTS	v2.2	~ 3–4 km	Jan 2005–Sep 2009
Aura MLS	v2.2	~ 2.5–3.0 km	Jan 2005–Apr 2012
Lidar: Hohenpeissenberg	V5.60 MOHP3	~ 1–2 km below 30 km; degrading to ~ 9 km above 40 km	Jul 2002–Mar 2012
Lidar: Lauder	v8.2	~ 1.8–3 km up to 30 km; degrading above	Jul 2002–Jun 2011
Lidar: Mauna Loa	v05.15	~ 2–3 km up to 40 km; degrading above	Jul 2002–Mar 2012
Lidar: Observatoire Haute Provence	v4	~ 0.6–2.4 km up to 30 km; degrading to ~ 6.5 km at 45 km	Jul 2002–Jan 2012
Lidar: Table Mountain	LidAna v05.4x to v6.x	~ 2–4 km up to 30 km; degrading above	Jul 2002–Jan 2012
Odin OSIRIS	v5.07	~ 2.2 km up to about 40 km; degrading above	Jul 2002–Apr 2012

ACPD
13, 17849–17900, 2013

Table 2. Summary of coincidence criteria and the total number of coinciding profiles (reduced time periods – January 2005 to April 2012 – in parenthesis) for the reference instruments with MIPAS showing the maximal time and spatial distance allowed between the measurements.

Instrument Instrument	Time criteria [h]	Distance criteria [km]	Number of coinciding profiles
ACE-FTS	24	1000	14 190
Aura MLS	6	250	401 251
Lidar: Hohenpeissenberg (2005–2012)	24	1000	652 (509)
Lidar: Lauder	24	1000	243
Lidar: Mauna Loa (2005–2012)	24	1000	693 (503)
Lidar: Observatoire Haute Provence	24	1000	753
Lidar: Table Mountain	24	1000	539
Odin OSIRIS (2005–2012)	6	250	109 820 (94 274)

ACPD
13, 17849–17900, 2013

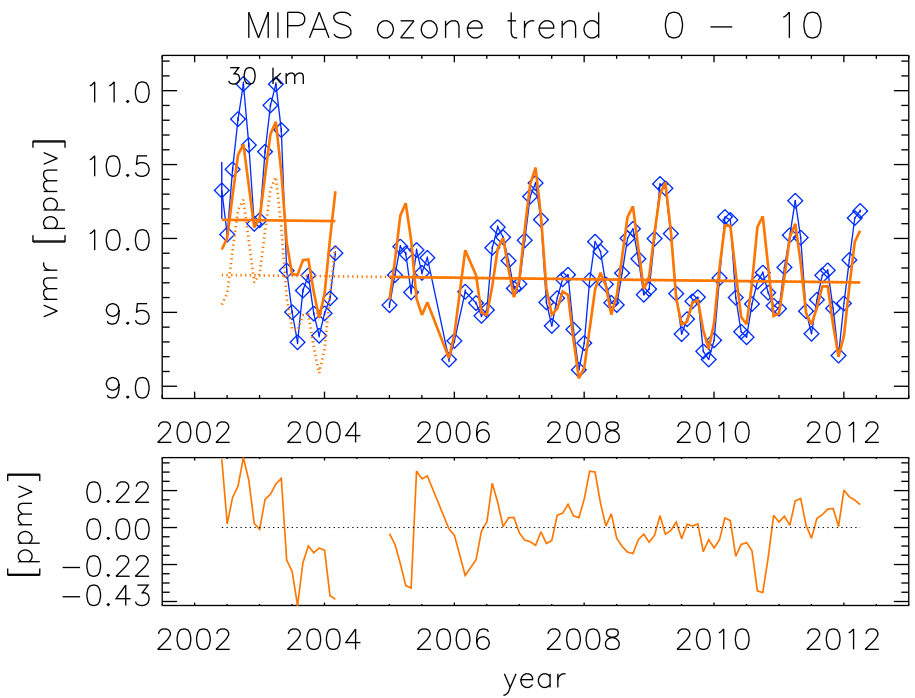

Fig. 1. Trendfit for 0 to 10° N, showing the monthly mean data (blue diamonds) the calculated fit and the related trend (orange lines) for MIPAS ozone measurements at 30 km. The dotted orange line represents the linear component of the regression function for times affected by bias correction. The bottom panel shows the residual of the fit and the data points.

ACPD
13, 17849–17900, 2013

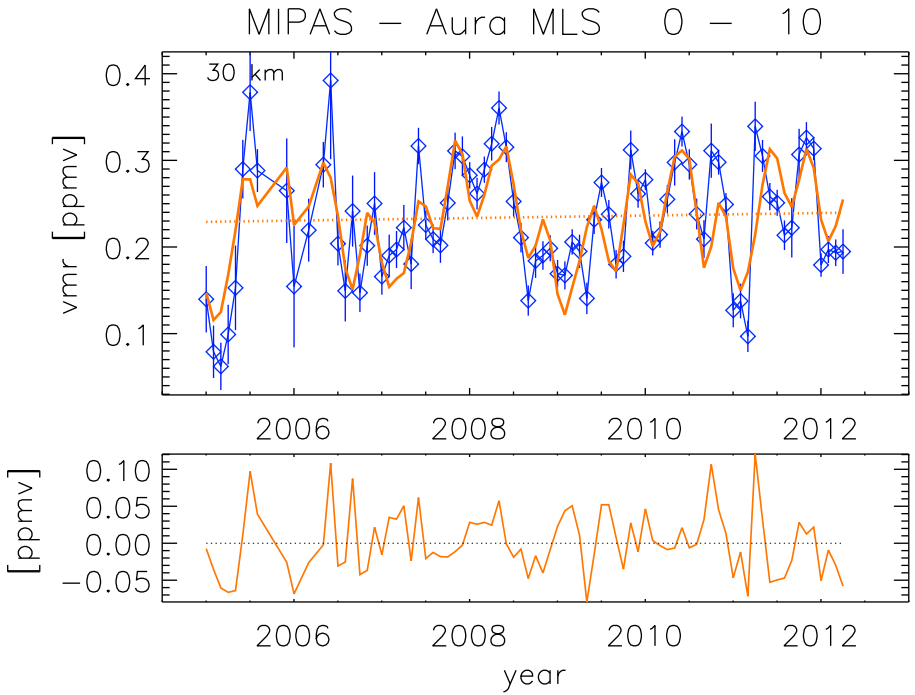

Fig. 2. Trendfit for 0 to 10° N, showing the monthly mean data (blue diamonds) the calculated fit and the related trend (orange lines) for the differences in the ozone measurements of MIPAS and Aura MLS at 30 km. The first subset of data is missing in the plot compared to Fig. 1, because Aura MLS and MIPAS have no overlap time within the first period of the MIPAS mission (cf. Table 1). The bottom panel shows the residual of the fit and the data points.

ACPD
13, 17849–17900, 2013

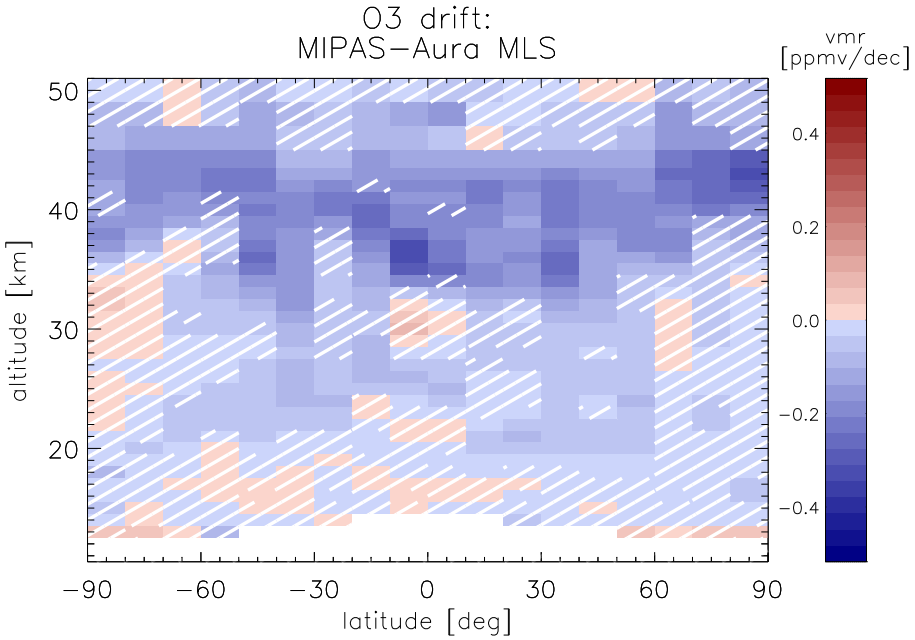

Fig. 3. Altitude-latitude cross-section of absolute drifts of MIPAS vs. Aura MLS ozone measurements. Hatched areas mean that the significance is less than 2 sigma.

ACPD
13, 17849–17900, 2013

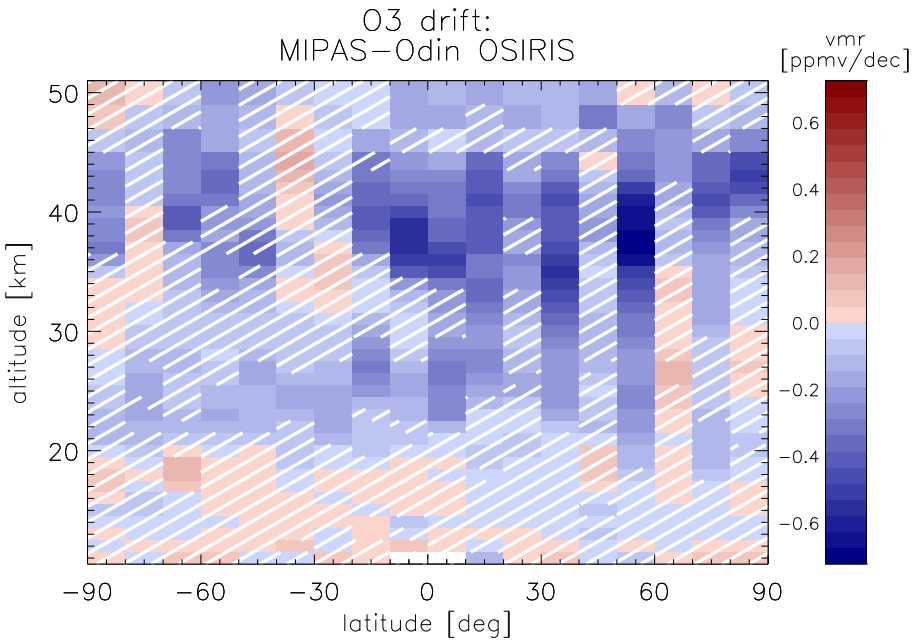

Fig. 4. Same as in Fig. 3 but for comparison versus Odin OSIRIS.

ACPD
13, 17849–17900, 2013

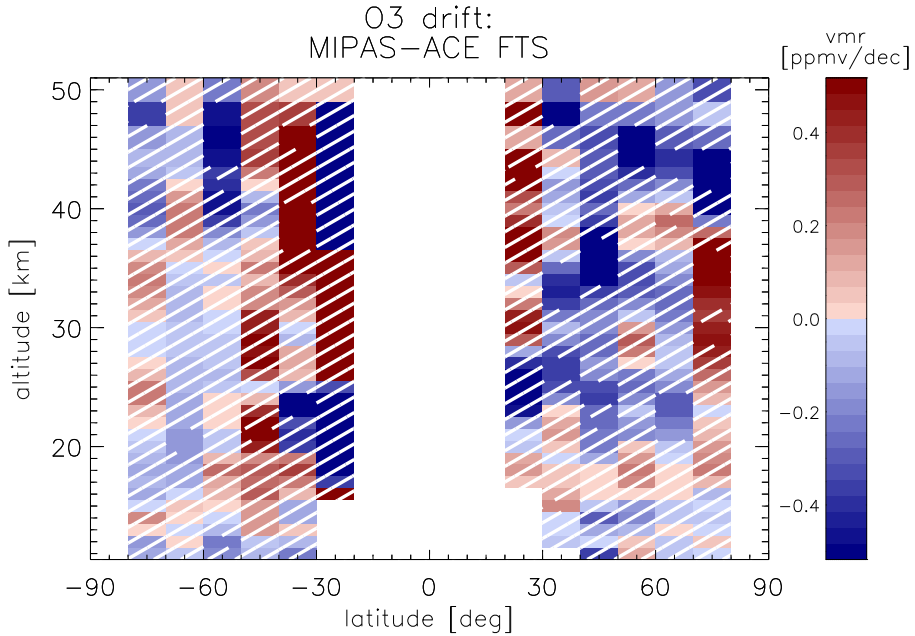

Fig. 5. Same as in Fig. 3 but for comparison versus ACE-FTS.

ACPD
13, 17849–17900, 2013

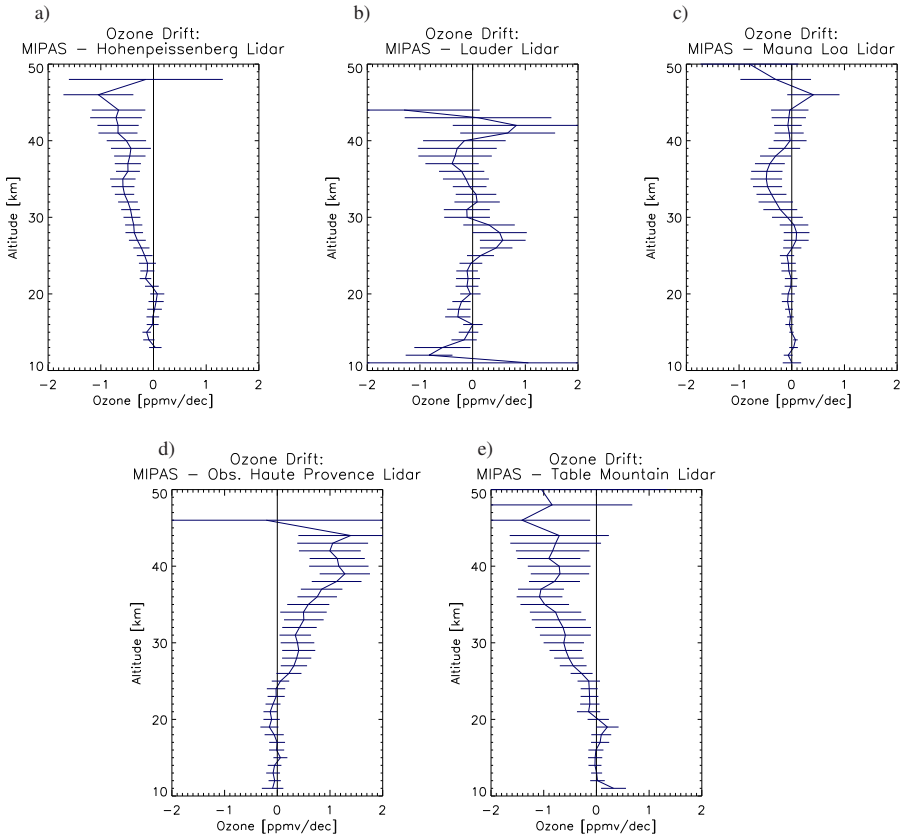

Fig. 6. Absolute drifts of MIPAS vs. **(a)** Hohenpeissenberg, **(b)** Lauder, **(c)** Mauna Loa, **(d)** Observatoire Haute Provence and **(e)** Table Mountain lidar ozone measurements. The error bars are the 2-sigma uncertainties of the estimated drifts.

ACPD
13, 17849–17900, 2013

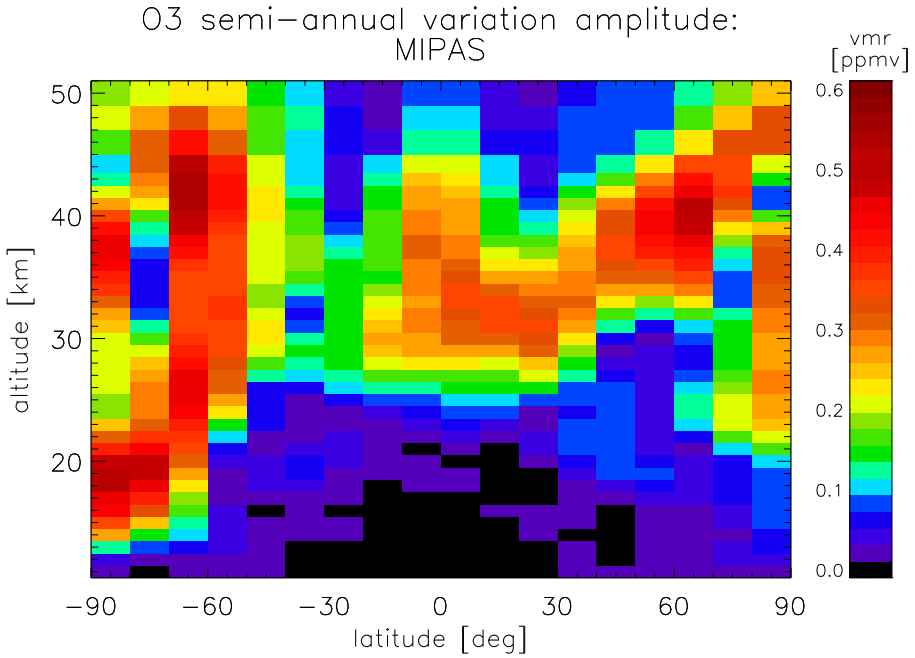

Fig. 7. Altitude-latitude cross-section of the amplitudes in ppmv of the semi-annual oscillation (6-month periodic variation) derived from the MIPAS time series.

ACPD
13, 17849–17900, 2013

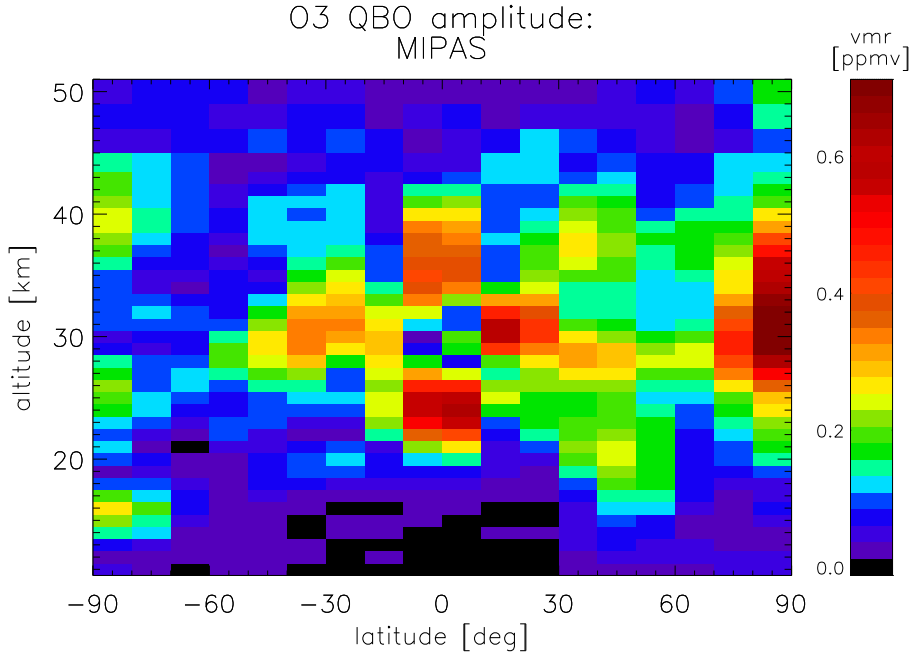

Fig. 8. Same as in Fig. 7, but for the quasi-biennial oscillation (QBO).

ACPD
13, 17849–17900, 2013

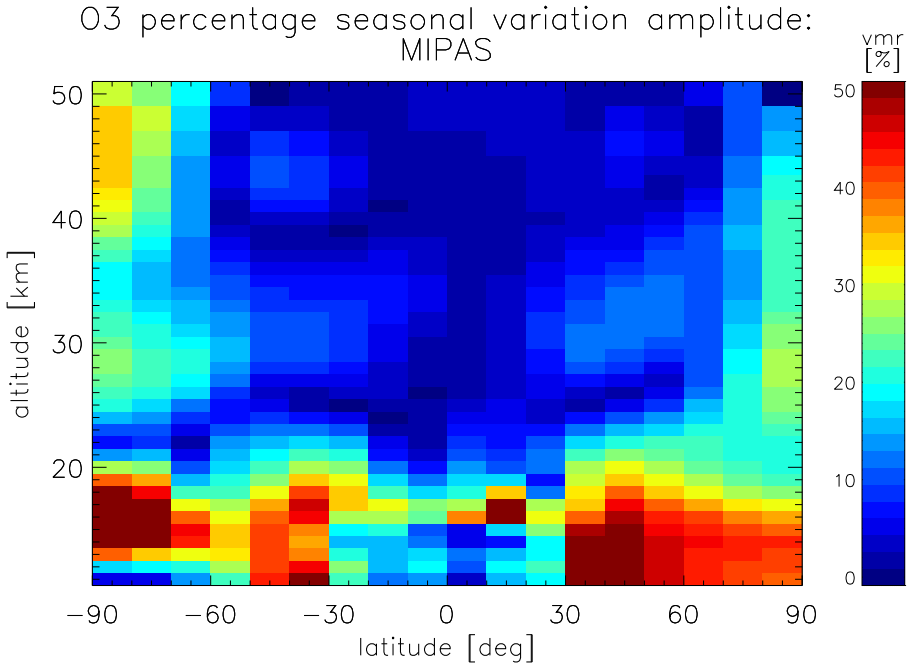

Fig. 9. Percentage amplitude of the seasonal variation of the MIPAS ozone time series (12 month periodic variation).

ACPD
13, 17849–17900, 2013

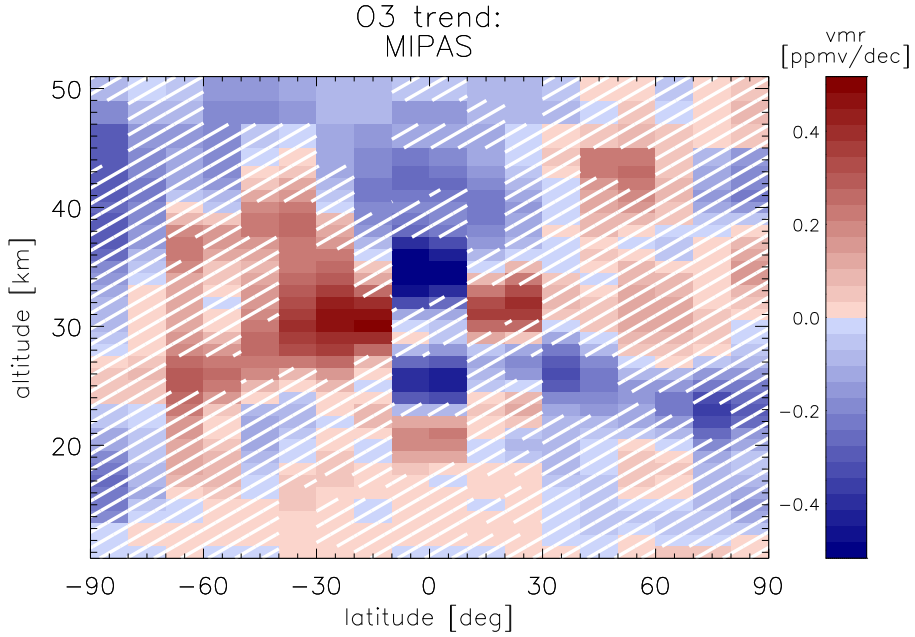

Fig. 10. Altitude-latitude cross-section of the linear variation of the MIPAS time series. As for the drifts, hatched areas indicate trends with less than 2 sigma significance level.

ACPD
13, 17849–17900, 2013

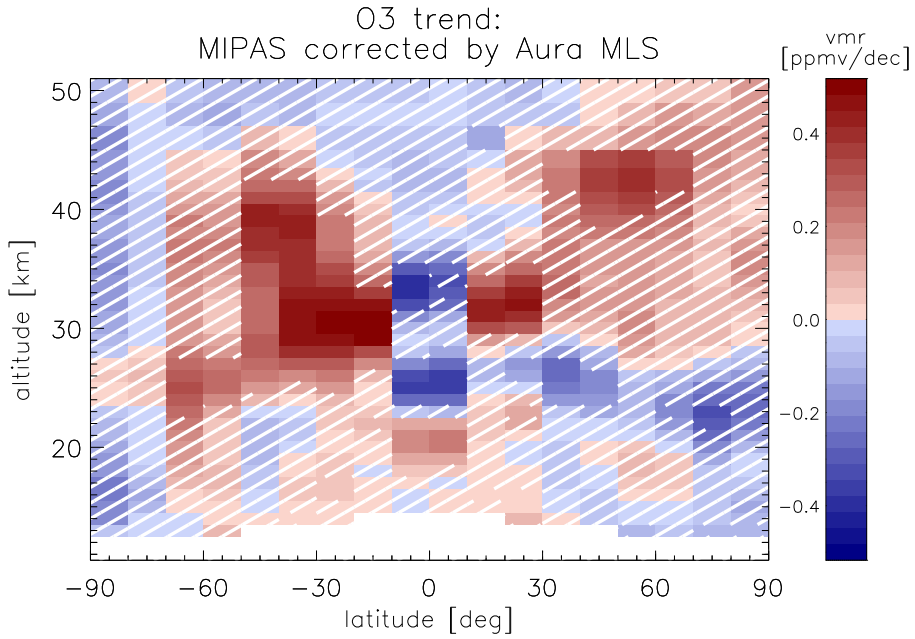

Fig. 11. Same as in Fig. 10 but corrected by the drifts estimated in comparison with Aura MLS. 2 sigma significances are based on the combined error of the trend and the drift.

ACPD
13, 17849–17900, 2013

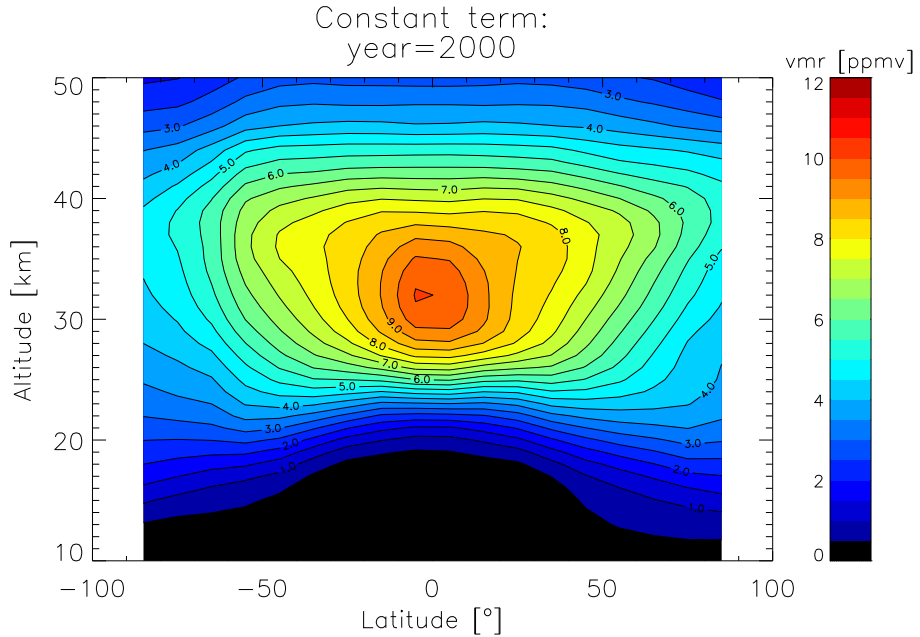

Fig. 12. Constant term of the trend estimation of the MIPAS ozone time series at the year 2000.

ACPD
13, 17849–17900, 2013

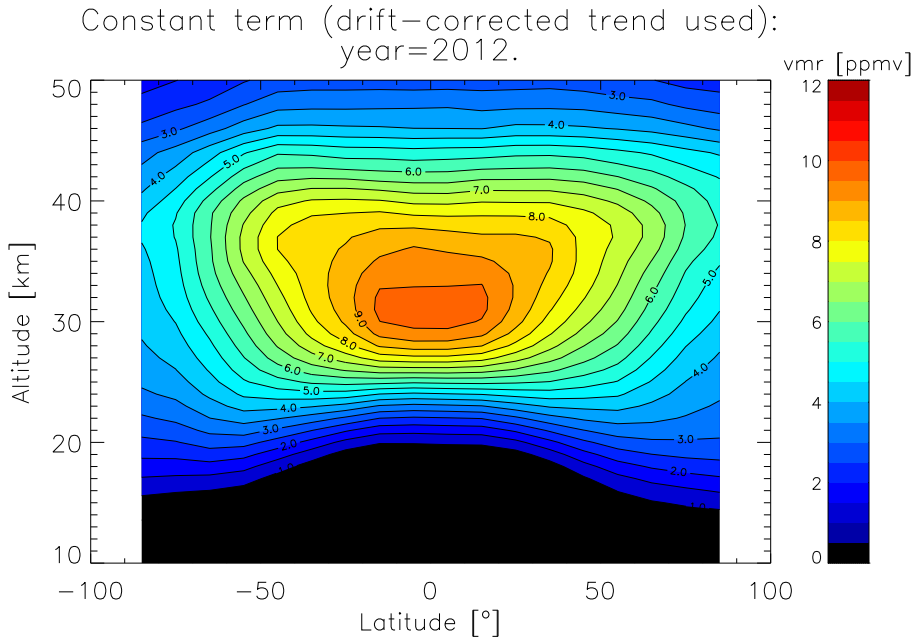

Fig. 13. Same as in Fig. 12, but for the year 2012. The MIPAS trend which was corrected by the drift estimated in comparison with Aura MLS was used to assess the constant term for the year 2012.

ACPD
13, 17849–17900, 2013

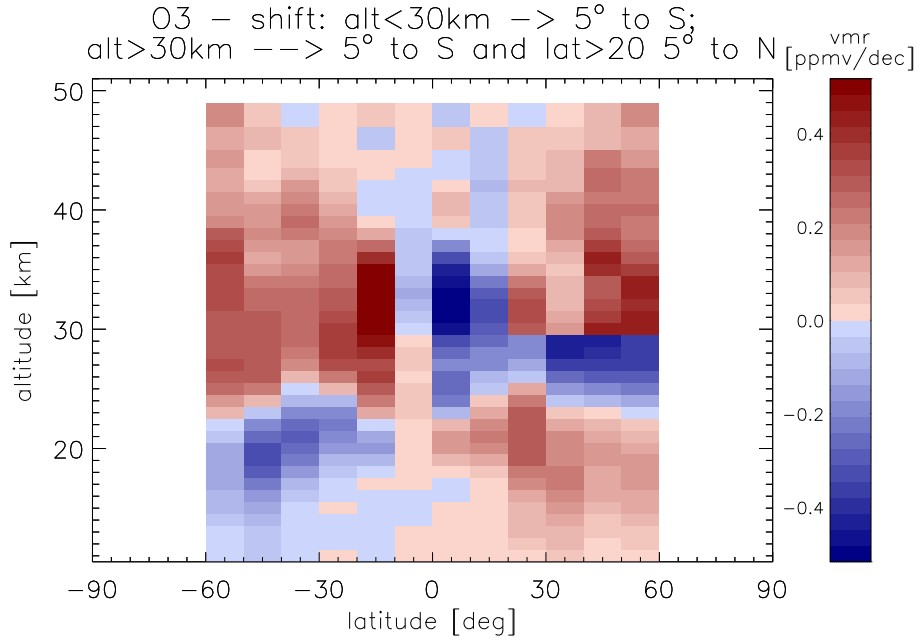

Fig. 14. Altitude-latitude cross-section showing the resulting trends when shifting the tropical mixing barriers below 30 km by 5° to the south and above expanding them by 5°.

ACPD
13, 17849–17900, 2013

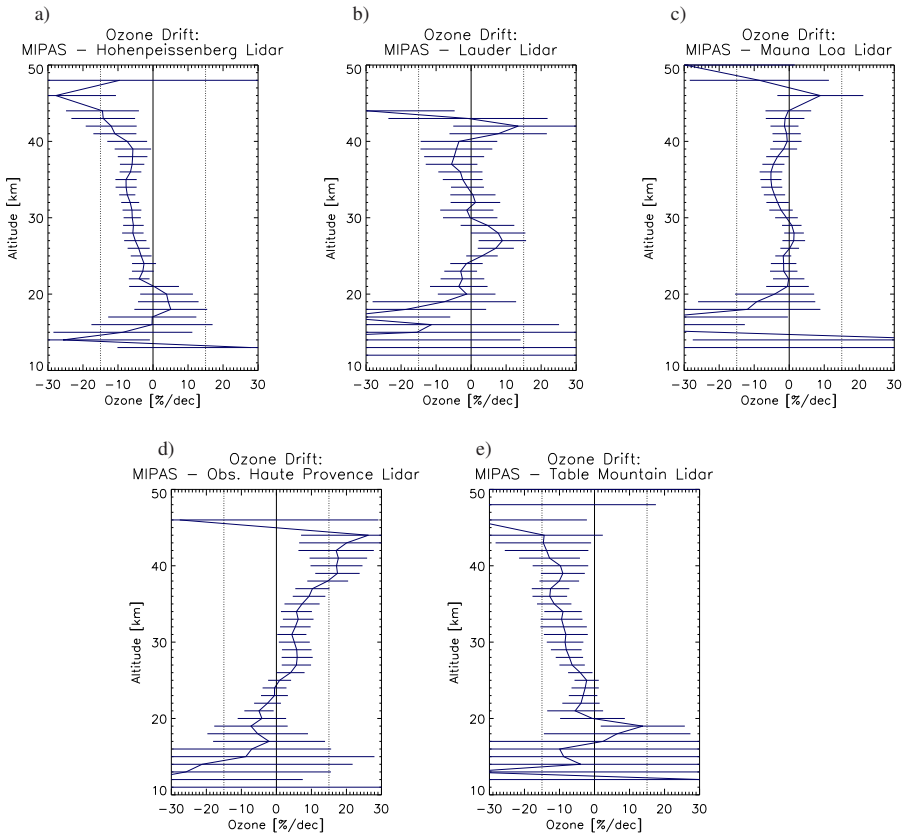

Fig. A1. Same as Fig. 6 but showing relative drifts.

ACPD
13, 17849–17900, 2013

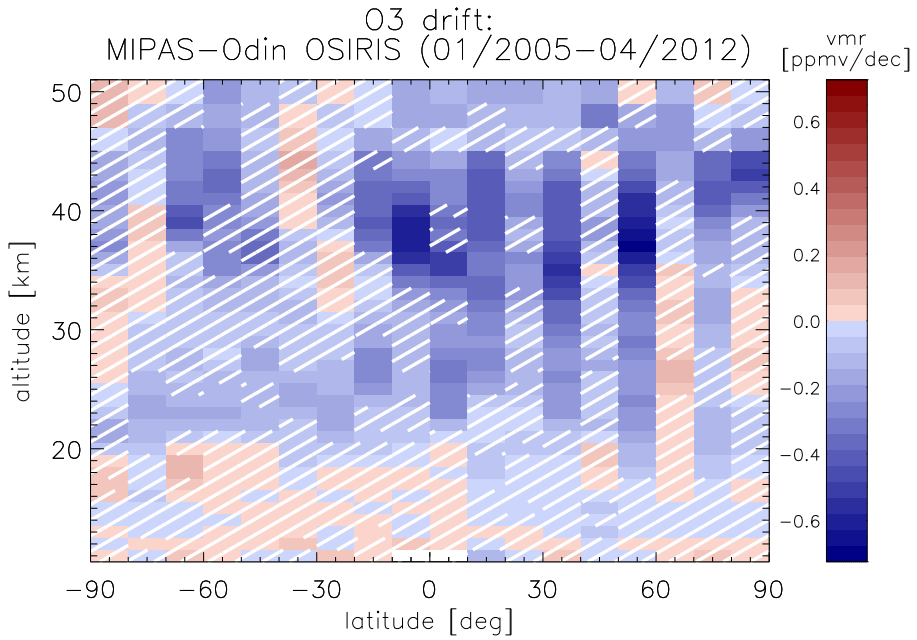

Fig. A2. Altitude-latitude cross-section of absolute drifts of MIPAS vs. Odin OSIRIS ozone measurements only for the time period from January 2005 to April 2012. Hatching as described before.

ACPD
13, 17849–17900, 2013

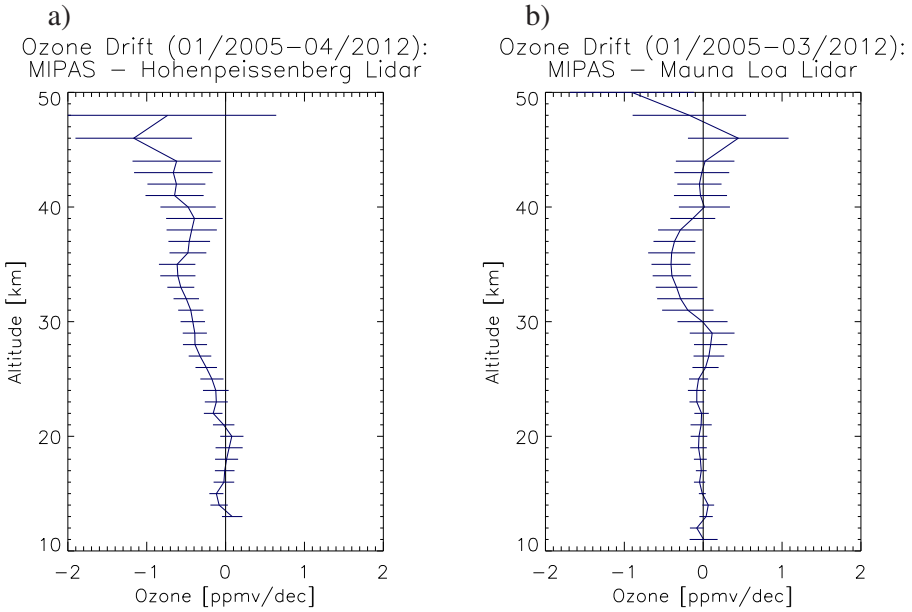

Fig. A3. Same as Fig. 6a and c but only for the time period of 2005 to 2012.

ACPD
13, 17849–17900, 2013